Mon. Not. R. Astron. Soc. **000**, 1–20 (2013) Printed 25 March 2013 (MN LaTeX style file v2.2)

arXiv:1303.5528v1 [astro-ph.GA] 22 Mar 2013

What determines the grain size distribution in galaxies?

Ryosuke S. Asano[1]⋆†, Tsutomu T. Takeuchi[1], Hiroyuki Hirashita[2], and Takaya Nozawa[3]
[1] *Department of Particle and Astrophysical Science, Nagoya University, Furo-cho, Chikusa-ku, Nagoya 464-8602, Japan*
[2] *Institute of Astronomy and Astrophysics, Academia Sinica, P. O. Box 23-141, Taipei 10617, Taiwan*
[3] *Kavli Institute for the Physics and Mathematics of the Universe, Todai Institutes for Advanced Study, the University of Tokyo, Kashiwa, Chiba 277-8583, Japan*

Accepted 2013 March 18. Received 2013 March 18; in original form 2012 December 28

ABSTRACT

Dust in galaxies forms and evolves by various processes, and these dust processes change the grain size distribution and amount of dust in the interstellar medium (ISM). We construct a dust evolution model taking into account the grain size distribution, and investigate what kind of dust processes determine the grain size distribution at each stage of galaxy evolution. In addition to the dust production by type II supernovae (SNe II) and asymptotic giant branch (AGB) stars, we consider three processes in the ISM: (i) dust destruction by SN shocks, (ii) metal accretion onto the surface of preexisting grains in the cold neutral medium (CNM) (called grain growth), and (iii) grain–grain collisions (shattering and coagulation) in the warm neutral medium (WNM) and CNM. We found that the grain size distribution in galaxies is controlled by stellar sources in the early stage of galaxy evolution, and that afterwards the main processes that govern the size distribution changes to those in the ISM, and this change occurs at earlier stage of galaxy evolution for a shorter star formation timescale (for star formation time-scales $= 0.5, 5$ and 50 Gyr, the change occurs about galactic age $t \sim 0.6, 2$ and 5 Gyr, respectively). If we only take into account the processes which directly affect the total dust mass (dust production by SNe II and AGB stars, dust destruction by SN shocks, and grain growth), the grain size distribution is biased to large grains ($a \sim 0.2$–0.5 μm, where a is the grain radius). Therefore, shattering is crucial to produce small ($a \lesssim 0.01$ μm) grains. Since shattering produces a large abundance of small grains (consequently, the surface-to-volume ratio of grains increases), it enhances the efficiency of grain growth, contributing to the significant increase of the total dust mass. Grain growth creates a large bump in the grain size distribution around $a \sim 0.01$ μm. Coagulation occurs effectively after the number of small grains is enhanced by shattering, and the grain size distribution is deformed to have a bump at $a \sim 0.03$–0.05 μm at $t \sim 10$ Gyr. We conclude that the evolutions of the total dust mass and the grain size distribution in galaxies are closely related to each other, and the grain size distribution changes considerably through the galaxy evolution because the dominant dust processes which regulate the grain size distribution change.

Key words: dust, extinction – galaxies: evolution – galaxies: ISM – ISM: clouds – galaxies: general – stars: formation

1 INTRODUCTION

Dust is one of the most important factors for the understanding of galaxy evolution. Since hydrogen molecules are efficiently formed on the surface of dust grains, the molecular formation rate is much larger than the case without dust. Such an enrichment of molecular abundance by dust realizes a favorable condition for star formation (e.g., Hirashita & Ferrara 2002). Dust grains also absorb stellar light mainly at ultraviolet and optical wavelengths and re-emit in the infrared. Consequently, dust affects the spectral energy distribution (SED) of galaxies (e.g., Takagi et al. 2003). Furthermore, the formation rate of hydrogen molecules on the grain surface and the mass absorption coefficient of radiation depend strongly on the grain size distribution (e.g., Hirashita & Ferrara 2002; Takeuchi et al. 2003).

⋆ E-mail: asano.ryosuke@g.mbox.nagoya-u.ac.jp
† Fellow of the Japan Society for the Promotion of Science (JSPS).

© 2013 RAS

Dust grains form by condensation of elements heavier than helium (i.e., metals). Metals are mainly supplied from asymptotic giant branch stars (AGB stars) and supernovae (SNe), and part of them condense into dust grains (e.g,. Mathis 1990). Dust grains are not only supplied by stars but are also destroyed by SN shocks in the interstellar medium (ISM) (e.g., Jones, Tielens & Hollenbach 1996; Nozawa et al. 2006; Zhukovska, Gail, & Trieloff 2008). Furthermore, it is thought that metal accretion onto the surface of grains in the ISM (referred to as "grain growth" in this paper) is an important process for explaining the amount of dust in the Milky Way (e.g., Draine 2009; Pipino et al. 2011). To the present day, there have been a lot of studies that investigate the evolution of the total dust mass in galaxies by taking into account these processes (e.g., Dwek & Scalo 1980; Dwek 1998; Hirashita 1999a,b; Inoue 2003, 2011; Calura, Pipino & Matteucci 2008; Zhukovska, Gail, & Trieloff 2008; Pipino et al. 2011; Asano et al. 2013). They assumed a representative grain size, but the efficiencies of dust destruction and grain growth depend on the grain size distribution. Thus, we should consider the evolution of the grain size distribution to understand the total dust mass precisely.

The grain size distribution is derived from observed extinction curves (which mainly depend on the grain size distribution and the grain species). According to Mathis, Rumpl & Nordsieck (1977), if spherical grains are assumed, the extinction curve in the Milky Way is reproduced by $f(a)\mathrm{d}a \propto a^{-3.5}\mathrm{d}a$ ($0.005 < a < 0.25$ μm; this grain size distribution is referred to as the MRN distribution), where a is the grain radius and $f(a)\mathrm{d}a$ is the number density of grains in size interval $[a, a + \mathrm{d}a]$ (see Kim, Martin, & Hendry 1994; Weingartner & Draine 2001, for more detailed fitting to the Milky Way extinction curve). The situation seems to be very different for distant galaxies. Recently, Gallerani et al. (2010) discussed the extinction curves of seven quasars at high redshift ($3.9 \leqslant z \leqslant 6.4$). They showed that these extinction curves tend to be flat at wavelengths < 0.2 μm in the quasar's rest frame. The difference between extinction curves in distant and nearby objects may indicate that different processes dominate the dust evolution at different epochs.

In young galaxies, Type II SNe (SNe II) are thought to be the dominant sources of dust because of short lifetime of their progenitors. However, Valiante et al. (2009) suggested that AGB stars are also important sources of dust production even at galactic age less than 1 Gyr. In addition, grain growth is expected to be the dominant process to increase dust mass in galaxies if the metallicity becomes larger than a certain value (Inoue 2011; Asano et al. 2013). Furthermore, if the metallicity reaches a sub-solar value, grain–grain collisions in the ISM (shattering and coagulation) become efficient enough to change the grain size distribution significantly (e.g., Hirashita & Yan 2009). We call all processes affecting the grain size distribution 'dust processes'.

These dust processes affect the different sizes of grains in galaxies. Nozawa et al. (2007) showed that SNe II supply relatively large grains ($a \gtrsim 0.01$ μm) into the ISM because small grains are destroyed by reverse shocks before they are ejected into the ISM (see also Bianchi & Schneider 2007; Silvia, Smith, & Shull 2012). The size distribution of grains produced by AGB stars is thought to be biased to large (~ 0.1 μm) sizes (e.g., Winters et al. 1997; Groenewegen 1997; Yasuda & Kozasa 2012). Furthermore, the smaller grains in the ISM are more easily destroyed by interstellar shocks driven by SNe (e.g., Nozawa et al. 2006). If grain growth occurs, since the timescale of this process is proportional to the volume-to-surface ratio of a grain, smaller grains grow more efficiently (e.g., Hirashita & Kuo 2011). After the dust grains are released into the diffuse ISM, shattering can also occur. Yan et al. (2004) showed that large grains ($a \gtrsim 0.1$ μm) acquire larger velocity dispersions than the shattering threshold velocity if the grains are dynamically coupled with magnetized interstellar turbulence. Shattering is indeed a promising mechanism of small–grain production (e.g., Hirashita 2010). Shattering also occurs in SN shocks (Jones, Tielens & Hollenbach 1996). In dense regions, coagulation can occur, so that the grain size distribution shifts to larger sizes (e.g., Ormel et al. 2009; Hirashita & Yan 2009). The various dust processes above in galaxies occur on timescales dependent on the metallicity, the total dust amount, the grain size distribution, and so on. Hence, it is crucial to consider all dust processes in a unified framework to understand the evolution of both the total dust amount and the grain size distribution.

There have been a number of studies on the evolution of the grain size distribution in galaxies. Liffman & Clayton (1989) discussed the evolution of grain size distribution considering dust destruction by SN shocks and grain growth. However, they did not consider shattering and coagulation by grain–grain collisions. O'Donnell & Mathis (1997) suggested a dust evolution model in a multi-phase ISM [warm neutral medium (WNM) and cold neutral medium (CNM)], and also considered the collisional processes of dust grains. However, they did not consider the size distribution of grains released by stars in order to simplify their model. Hirashita et al. (2010) discussed the grain size distribution in young starburst galaxies. They assumed that SNe II are the source of dust in these galaxies and focused on the production of small grains by shattering. Yamasawa et al. (2011) constructed a dust evolution model taking into account dust formation and destruction by SNe II along with the formation and evolution of galaxies. However, since they focused on galaxies in the high-z Universe, they did not consider dust formation in AGB stars, grain growth, shattering and coagulation.

In this work, we construct a dust evolution model taking into account the dust formation by SNe II and AGB stars, dust destruction by SN shocks, grain growth, and shattering and coagulation, to investigate what kind of dust processes determine the grain size distribution at each stage of galaxy evolution. In our model, we do not consider mass exchange among various ISM phases in detail (e.g., Ikeuchi & Tomita 1983), but our results contain the contributions of dust processes in the two ISM phases, WNM (~ 6000 K, $0.3\ \mathrm{cm}^{-3}$) and CNM (~ 100 K, $30\ \mathrm{cm}^{-3}$) by assuming these mass fractions in the ISM to be constant.

This paper is organized as follows: in Section 2 we introduce the dust evolution model based on chemical evolution of galaxies. In Section 3 we examine the contribution of each dust process to the grain size distribution. Section 4 is devoted to the discussion on what kind of dust processes regulate the grain size distribution in galaxies. We conclude this work in Section 5. Throughout this paper the solar metallicity is set to be $Z_\odot = 0.02$ (Anders & Grevesse 1989).

2 GALAXY EVOLUTION MODEL

In this Section, we introduce our dust evolution model in a galaxy. First, we show the basic equations of the chemical evolution model. We then describe the dust evolutions based on the chemical evolution model, involving dust production by SNe II and AGB stars, dust destruction by SN shocks, grain growth, and shattering and coagulation by grain–grain collisions.

Some grain processing mechanisms work in a different way in a different ISM phase (O'Donnell & Mathis 1997). In this work, while we use a one-zone model to examine the representative properties of a galaxy, we consider the effects of the dust processes in WNM and CNM by introducing the mass fractions of WNM and CNM, $\eta_{\rm WNM}$ and $\eta_{\rm CNM}$. Considering temperatures less than 10^4 K, we find that an equilibrium state of two thermally stable phases (WNM and CNM) is established in the ISM (e.g., Wolfire et al. 2003). Thus, we calculate dust evolution taking into account a two-phase neutral ISM. We also assume that the galaxy is a closed-box; that is, the total baryon mass $M_{\rm tot}$ (the sum of the stellar mass and the ISM mass in the galaxy) is constant. Since $M_{\rm tot}$ is just a scale factor in our work, the total dust mass just scales with $M_{\rm tot}$. Throughout this paper $M_{\rm tot}$ is set to be 10^{10} $\rm M_{\odot}$.

Inflow and outflow are not considered in our model for simplicity. Since inflowing gas is considered to be not only metal poor but also dust poor, the abundance of both metals and dust are diluted with the same (or similar) fraction by inflow. This effect is degenerate with a slower chemical enrichment, under a longer $\tau_{\rm SF}$, where $\tau_{\rm SF}$ is the star formation timescale. As for outflow, since ISM components (namely gas, metals, and dust) are blown out of a galaxy, the total gas mass in a galaxy decreases. In this case, star formation rate decreases at earlier phase of galaxy evolution; that is, the effect of outflow is degenerate with a shorter $\tau_{\rm SF}$. Thus, we just absorb the effects of inflow and outflow into $\tau_{\rm SF}$.

2.1 Chemical evolution model

In this subsection, we describe our model of chemical evolution in a galaxy. From the above assumptions, the equations of time evolution of the total stellar mass, M_*, the ISM mass, $M_{\rm ISM}$, and the mass of a metal species X, $M_{\rm X}$, in the galaxy are expressed as

$$\frac{{\rm d}M_*(t)}{{\rm d}t} = {\rm SFR}(t) - R(t), \tag{1}$$

$$\frac{{\rm d}M_{\rm ISM}(t)}{{\rm d}t} = -{\rm SFR}(t) + R(t), \tag{2}$$

$$\frac{{\rm d}M_{\rm X}(t)}{{\rm d}t} = -Z_{\rm X}(t){\rm SFR}(t) + Y_{\rm X}(t), \tag{3}$$

where t is the galaxy age, SFR(t) is the star formation rate, $Z_{\rm X} = M_{\rm X}/M_{\rm ISM}$, and $R(t)$ and $Y_{\rm X}(t)$ are the masses of the total baryons and total metal species X released by stars in a unit time, respectively. In this paper, we consider two dust species, carbonaceous dust and silicate dust, and we adopt two key elements of dust species (X = C for carbonaceous dust and X = Si for silicate dust) in calculating dust evolution (see Section 2.2 for details). We adopt $M_*(0) = 0$, $M_{\rm ISM}(0) = M_{\rm tot}$, and $M_{\rm X}(0) = 0$ as initial conditions.

In our work, we adopt the Schmidt law for the SFR: SFR $\propto M_{\rm ISM}^n$ (Schmidt 1959), and the index n is thought to be 1–2 observationally (e.g., Kennicutt 1998). We here adopt $n = 1$,

$${\rm SFR}(t) = \frac{M_{\rm ISM}(t)}{\tau_{\rm SF}}, \tag{4}$$

where the star formation timescale $\tau_{\rm SF}$ is a constant. For comparison, the case with $n = 1.5$ is also shown in Appendix A1. As long as we adopt the same star formation timescale at $t = 0$, there is little difference between the two cases with $n = 1$ and 1.5.

$R(t)$ and $Y_{\rm X}(t)$ are written as

$$R(t) = \int_{m_{\rm cut}(t)}^{100\ {\rm M_{\odot}}} \left[m - \omega(m, Z(t-\tau_m))\right] \phi(m){\rm SFR}(t){\rm d}m, \tag{5}$$

$$Y_{\rm X}(t) = \int_{m_{\rm cut}(t)}^{100\ {\rm M_{\odot}}} m_{\rm X}(m, Z(t-\tau_m))\phi(m){\rm SFR}(t){\rm d}m, \tag{6}$$

where $\phi(m)$ is the stellar initial mass function, τ_m is the lifetime of a star with mass m at the zero-age main sequence, Z is the metallicity ($= \Sigma_X M_{\rm X}/M_{\rm ISM}$), and $\omega(m, Z)$ and $m_{\rm X}(m, Z)$ represent the mass of remnant stars (white dwarfs, neutron stars or black holes) and the mass of metal species X ejected by a star of mass m and metallicity Z, respectively. For the lifetime of stars, we adopt the formula derived by Raiteri, Villata & Navarro (1996), and the formula is obtained by the fitting to the stellar models of the Padova group (Bertelli et al. 1994). Since its metallicity dependence is weak, we always adopt the stellar lifetime for solar metallicity as a representative value. The lower bound of the integration, $m_{\rm cut}(t)$ is the mass of a star with $\tau_m = t$. We adopt the Salpeter IMF for stellar mass range 0.1–100 $\rm M_{\odot}$ (Salpeter 1955):

$$\phi(m) \propto m^{-q}, \tag{7}$$

where q is set to be 2.35, and the normalization is determined by

$$\int_{0.1\ {\rm M_{\odot}}}^{100\ {\rm M_{\odot}}} m\phi(m){\rm d}m = 1. \tag{8}$$

Table 1. parameters for each dust species

Species	X	$g_{\rm X}$	$m_{\rm X}$ [amu]	s [g cm^{-3}] $^{\rm b}$	$v_{\rm shat}$ [km s^{-1}]	γ [erg cm^{-2}] $^{\rm c}$	E [dyn cm^{-2}] $^{\rm c}$	ν $^{\rm c}$
Graphite	C	1.0	12	2.26	1.2	75	1.0×10^{11}	0.32
Silicate	Si	0.166 $^{\rm a}$	28.1	3.3	2.7	25	5.4×10^{11}	0.17

Note. X is the key element of dust species, $g_{\rm X}$ is the mass fraction of the key element X in the grains, $m_{\rm X}$ is the atomic mass of X, s is the bulk density of dust grains, $v_{\rm shat}$ is the shattering threshold velocity, γ is the surface energy per unit area of grains, E is Young's modulus, and ν is Poisson's ratio.

[a] We assume $\rm Mg_{1.1}Fe_{0.9}SiO_4$ for the composition of silicate (Draine & Lee 1984).

[b] Draine & Lee (1984).

[c] Chokshi, Tielens, & Hollenbach (1993).

To check the variation of the results with q, we examine the case with $q = 1.35$ (a top heavy IMF) in Appendix A2. For $q = 1.35$, the processes in the ISM occur at earlier phases of galaxy evolution than for $q = 2.35$, because a larger amount of dust is supplied by stars. However, we find that the sequence of the dominant dust processes along the age does not change so the following discussions are not altered significantly by the change of q. Thus, we only consider $q = 2.35$ in the following discussion.

To calculate Eqs. (5) and (6), we quote the remnant and metal mass data of stars with mass m and metallicity Z from some previous works. We assume that the mass ranges of AGB stars and SNe II are 1–8 $\rm M_\odot$ and 8–40 $\rm M_\odot$, respectively, and that all stars with initial masses more than 40 $\rm M_\odot$ evolve into black holes without ejecting any gas, metals or dust (Heger et al. 2003). The data for AGB stars with mass 1–6 $\rm M_\odot$ and metallicity $Z = (0.005, 0.2, 0.4, 1.0)$ $\rm Z_\odot$ is taken from Karakas (2010) and the data for SNe II with mass 13–40 $\rm M_\odot$ and metallicity $Z = (0.0, 0.05, 0.2, 1.0)$ $\rm Z_\odot$ is from Kobayashi et al. (2006). We interpolate and extrapolate the data for all values of mass and metallicity (also for the dust data in Sections 2.2.1 and 2.2.2).

2.2 Dust evolution

For dust evolution, we consider dust production by SNe II and AGB stars, dust destruction by SN shocks in the ISM, grain growth in the CNM, and shattering and coagulation by grain–grain collisions in the WNM and CNM. In this work, as mentioned in Section 1, we assume a two-phase ISM (WNM and CNM) to calculate the dust evolution (see also Section 2.2.5).

We neglect the contribution of Type Ia SNe (SNe Ia) to the production of metals and dust, and the destruction of dust. Nozawa et al. (2011) showed that SNe Ia release little dust into the ISM. Furthermore, dust destruction by SNe Ia is expected to be insignificant to the total dust budget in galaxies (less than 1/10 of the contribution of SNe II; Calura, Pipino & Matteucci (2008)). As for metals, although Nomoto et al. (1997) showed that the contribution of SNe Ia to the silicon and carbon enrichment in the ISM can be comparable to that of SNe II, the ratio between SN Ia rate and SN II rate is unknown [Nomoto et al. (1997) suggested that it is about 0.1 taking into account a chemical evolution model]. Thus, to simplify the discussion, we neglect the contribution from SNe Ia, keeping in mind a possible underproduction of metallicity.

The dust production data we adopt contain a lot of dust species (C, Si, $\rm SiO_2$, SiC, Fe, FeS, $\rm Al_2O_3$, MgO, $\rm MgSiO_3$, $\rm FeSiO_3$, $\rm Mg_2SiO_4$, and $\rm Fe_2SiO_4$) (Nozawa et al. 2007; Zhukovska, Gail, & Trieloff 2008). However, the physical properties of grain species other than carbonaceous and silicate grains are not fully known. Hence, we categorize all grain species other than carbonaceous dust as silicate and calculate their growth, shattering, and coagulation by adopting the physical parameters of silicate grains. In particular, after grain growth and coagulation occur, the dust species categorized as silicate dust do not evolve separately and our simplification can avoid the complexity arising from the compound species. In fact, the mass of dust grains ejected by SNe is dominated by Si grains, which would grow into silicate grains in the oxygen-rich environments such as molecular clouds. For carbonaceous dust, we adopt material properties of graphite. The adopted parameters of these two grain species are shown in Table 1 and are the same as in Hirashita & Yan (2009) and Kuo & Hirashita (2012). Although we calculate silicate and carbonaceous dust separately, we are interested in how the overall grain size distribution is affected by each dust process. Therefore, we focus on the total grain size distribution.

In this work, we assume that grains are spherical. Thus, the mass of a grain with radius a is

$$m(a) = \frac{4\pi a^3}{3} s, \tag{9}$$

where s is the bulk density of dust grains. In our model, we consider that the minimum and maximum radii of grains, $a_{\rm min}$ and $a_{\rm max}$, are 0.0003 μm and 8 μm, respectively. Although the minimum size of grains is poorly known, even if $a_{\rm min} = 0.001$ μm, the evolution of both the total dust mass and the grain size distribution does not change significantly (Hirashita 2012).

2.2.1 *Dust production by AGB stars*

The size distribution of grains produced by AGB stars is not well known. Winters et al. (1997) suggested that the size distribution is log-normal with a peak at ~ 0.1 μm based on the fitting to observed SEDs. Yasuda & Kozasa (2012) have recently calculated the size distribution of SiC produced by C-rich AGB stars by performing dust formation calculation coupled with a hydrodynamical model. They showed that the mass distribution, $a^4 f(a)$, is close to log-normal with a peak at 0.2–0.3 μm, where the grain size distribution $f(a)$ is defined so that $f(a)\mathrm{d}a$ is the number density of dust grains with radii in the range $[a, a + \mathrm{d}a]$ (The size distribution multiplied by a^4 means the mass distribution per logarithmic grain radius). Hence, both theory and observations suggest that AGB stars preferentially produce large grains ($a \gtrsim 0.1$ μm). In this paper, we simply assume that the mass distribution, $a^4 f(a)$, of each species produced by AGB stars is log-normal with a peak at 0.1 μm with standard deviation $\sigma = 0.47$, so that the shape of the mass distribution in Fig. 7 in Yasuda & Kozasa (2012) is reproduced. We normalize $f(a)$ by

$$m_{\mathrm{d}}(m) = \int_0^\infty \frac{4\pi}{3} a^3 s f(a) \mathrm{d}a, \tag{10}$$

where $m_{\mathrm{d}}(m)$ is the dust mass released by a star with mass m. The size distributions of all species are assumed to be the same for simplicity. Dust mass data for AGB stars with mass 1–7 $\mathrm{M}_\odot$ and metallicity $Z = (5.0 \times 10^{-2}, 0.1, 0.2, 0.4, 0.75, 1.0)$ $\mathrm{Z}_\odot$ is taken from Zhukovska, Gail, & Trieloff (2008). The size distributions of dust species other than carbonaceous dust are summed to compose the grain size distribution of silicate (the same procedure is also applied in Section 2.2.2). We define $f_{\mathrm{X}}(a)$ as the size distribution of dust species, where X represents the key element of dust species (X = C for carbonaceous dust and X = Si for silicate dust).

2.2.2 *Dust production by SNe II*

Some fraction of dust grains in galaxies are produced in the ejecta of SNe II (e.g., Matsuura et al. 2011). After a SN explosion, reverse shock occurs because of interactions between the ISM surrounding the SN and its ejecta, and dust grains are destroyed by sputtering in the shock (e.g., Bianchi & Schneider 2007; Nozawa et al. 2007). Nozawa et al. (2007) calculated the total mass and size distribution of dust grains ejected by SNe II considering the dust destruction in the radiative and non-radiative phases of SN remnants. We adopt the data for dust mass and size distribution derived by Nozawa et al. (2007) for SNe II with mass 13–30 $\mathrm{M}_\odot$ [1]. They also considered two cases for mixing in the helium core: unmixed and mixed models. Hirashita et al. (2005) showed that the data from the unmixed model is in better agreement with observations than that of the mixed model. Hence, we adopt the unmixed model. Nozawa et al. (2007) showed that the size distribution of grains supplied by SNe II is biased to large (~ 0.1 μm) grains due to the destruction of small grains by the reverse shock.

The amount and size distribution of grains injected by SNe II depend on the density of the surrounding ISM because the dust destruction efficiency of the reverse shock is higher in the denser ISM. However, the trend that smaller grains are more easily destroyed does not change. In this paper, the hydrogen number density of the ISM surrounding the SNe II, n_{SN}, is set to be $1.0\ \mathrm{cm}^{-3}$ as a fiducial value, but the cases with $n_{\mathrm{SN}} = 0.1$ and $10.0\ \mathrm{cm}^{-3}$ are also examined.

2.2.3 *Dust destruction by SN shocks in the ISM*

Dust grains in the ISM are destroyed or become smaller by sputtering due to the passage of interstellar shocks driven by SNe. Since the destruction changes and depends on the grain size, it is important to consider dust destruction taking into account the grain size distribution.

To calculate this destruction process, we adopt the formulae in Yamasawa et al. (2011), which we show here briefly. The number density of dust grains with radii in the range $[a, a + \mathrm{d}a]$ after the passage of a SN shock, $f'_{\mathrm{X}}(a)\mathrm{d}a$, is given by

$$f'_{\mathrm{X}}(a)\mathrm{d}a = \int_a^\infty \xi_{\mathrm{X}}(a, a')\mathrm{d}a f_{\mathrm{X}}(a')\mathrm{d}a', \tag{11}$$

where $\xi_{\mathrm{X}}(a, a')\mathrm{d}a$ is the number fraction of grains that are eroded from the initial radii $[a', a' + \mathrm{d}a']$ to radii $[a, a + \mathrm{d}a]$ by sputtering in the SN shock and has been obtained using the models by Nozawa et al. (2006). Note that if $a > a'$, $\xi_{\mathrm{X}}(a, a') = 0$. Thus, the change in the number density of grains with radii $[a, a + \mathrm{d}a]$, $\mathrm{d}N_{\mathrm{d,X}}(a)$, after the passage of a single SN shock is expressed as

$$\mathrm{d}N_{\mathrm{d,X}}(a) = \int_0^\infty \xi_{\mathrm{X}}(a, a')\mathrm{d}a f_{\mathrm{X}}(a')\mathrm{d}a' - f_{\mathrm{X}}(a)\mathrm{d}a. \tag{12}$$

Accordingly, the change of mass density, $\mathrm{d}M_{\mathrm{d,X}}(a)$, is

$$\begin{aligned} \mathrm{d}M_{\mathrm{d,X}}(a) &= \frac{4}{3}\pi a^3 s \mathrm{d}N_{\mathrm{d,X}}(a) \\ &= \int_0^\infty \frac{4\pi a^3 s}{3} \xi_{\mathrm{X}}(a, a')\mathrm{d}a f_{\mathrm{X}}(a')\mathrm{d}a' - \mathcal{M}_{\mathrm{d,X}}(a)\mathrm{d}a, \end{aligned} \tag{13}$$

where $\mathcal{M}_{\mathrm{d,X}}(a)\mathrm{d}a = \frac{4}{3}\pi a^3 s f_{\mathrm{X}}(a)\mathrm{d}a = M_{\mathrm{d,X}}(a)$ is the total dust mass with radii $[a, a + \mathrm{d}a]$ before the dust destruction. The dust destruction efficiency $\xi_{\rm X}$ depends on the hydrogen number density of the ISM, $n_{\rm SN}$, such that dust grains are destroyed more efficiently in denser regions. As mentioned in Section 2.2.2, $n_{\rm SN} = 1.0 \ {\rm cm}^{-3}$ as a fiducial value in this paper.

---

[1] Although Nozawa et al. (2007) investigated only the dust formation in SNe II evolving from zero-metallicity stars, the grain species formed in the ejecta of SNe II and their size distribution are insensitive to the metallicity of progenitor stars (e.g., Todini & Ferrara 2001; Kozasa et al. 2009). In addition, the destruction efficiiency of dust by the reverse shocks is almost independent of metallicity in the ISM; its difference between $Z = 0$ and $Z = Z_\odot$ is less than 15% (see Nozawa et al. 2007).

The equation for the time evolution of $M_{\rm d,X}(a,t)$ for dust destruction by SN shocks in the ISM is expressed as

$$\frac{{\rm d}M_{\rm d,X}(a,t)}{{\rm d}t} = -\frac{M_{\rm swept}}{M_{\rm ISM}(t)}\gamma_{\rm SN}(t)\left[M_{\rm d,X}(a,t) - m(a)\int_0^\infty \xi_{\rm X}(a,a^{'}){\rm d}af_{\rm X}(a^{'},t){\rm d}a^{'}\right], \tag{14}$$

where $\gamma_{\rm SN}(t)$ is the SN rate and $M_{\rm swept}$ is the ISM mass swept up by a SN shock. To express the dependence on the galaxy age, we write $M_{\rm d,X}(a)$ and $f_{\rm X}(a)$ as $M_{\rm d,X}(a,t)$ and $f_{\rm X}(a,t)$, respectively.

The SN rate, $\gamma_{\rm SN}(t)$, is expressed as

$$\gamma_{\rm SN}(t) = \int_{8\ {\rm M}_\odot}^{40\ {\rm M}_\odot} \phi(m){\rm SFR}(t-\tau_m){\rm d}m, \tag{15}$$

where we assume that the range of integration in Eq. (15) is the mass range where SNe occur (Heger et al. 2003) (if $t - \tau_m < 0$, ${\rm SFR}(t-\tau_m) = 0$).

The ISM mass swept up by a SN shock, $M_{\rm swept}$, depends on the density and metallicity of the ISM. In our model, we adopt the following formula used in Yamasawa et al. (2011);

$$\frac{M_{\rm swept}}{M_\odot} = 1535 n_{\rm SN}^{-0.202}\left[\left(\frac{Z}{Z_\odot}\right) + 0.039\right]^{-0.289}. \tag{16}$$

2.2.4 *Grain growth*

Here, we formulate the growth process of grains taking into account the grain size distribution. In the ISM, particularly in dense and cold regions, metals accrete onto the surface of grains efficiently (e.g., Liffman & Clayton 1989; Inoue 2003; Draine 2009). Recently, various studies have shown the importance of grain growth for dust enrichment in galaxies (e.g., Zhukovska, Gail, & Trieloff 2008; Michałowski et al. 2010; Pipino et al. 2011; Valiante et al. 2011; Hirashita & Kuo 2011). Hirashita & Kuo (2011) showed quantitatively that the grain size distribution has a very important consequence for grain growth. Here, we follow the formulation by Hirashita & Kuo (2011) and consider only grain growth of refractory dust (silicate and carbonaceous dust in this paper). Although volatile grains such as water ice also exists in clouds in reality, they evaporate quickly when the clouds disappear or the gas temperature rises.

For grain growth, the following equation holds:

$$\frac{\partial f_{\rm X}(a,t)}{\partial t} + \frac{\partial}{\partial a}[f_{\rm X}(a,t)\dot{a}] = 0, \tag{17}$$

where $\dot{a} \equiv {\rm d}a/{\rm d}t$ is the growth rate of the grain radius [2].

From Eq. (9),

$$\frac{{\rm d}m(a)}{{\rm d}a} = 4\pi a^2 s. \tag{18}$$

Also, from Hirashita & Kuo (2011), the rate of mass increase of a grain with radius a is expressed as

$$\frac{{\rm d}m(a)}{{\rm d}t} = g_{\rm X}^{-1} m_{\rm X}\alpha\mathcal{R}, \tag{19}$$

where $g_{\rm X}$ is the mass fraction of the key species X in the grains, $m_{\rm X}$ is the atomic mass of X, α is the sticking coefficient of the key species, and $\mathcal{R}$ is the collision rate of X to a grain with radius a, defined as follows (Evans 1994)

$$\mathcal{R} = 4\pi a^2 n_{\rm X}(t)\left(\frac{kT_{\rm gas}}{2\pi m_{\rm X}}\right)^{1/2}, \tag{20}$$

where $n_{\rm X}(t)$ is the number density of X in the gas phase in the CNM, k is the Boltzmann constant, and $T_{\rm gas}$ is the gas temperature in the CNM. We apply $g_{\rm X} = 1.0$ and 0.166 for carbonaceous and silicate dust, respectively (Table 1) and $T_{\rm gas} = 100$ K.

Next, we consider $n_{\rm X}(t)$, which is evaluated by

$$n_{\rm X}(t) = \frac{\rho_{\rm ISM}^{\rm eff}}{m_{\rm X}}\frac{M_{\rm X}(t)}{M_{\rm ISM}(t)}\left[1 - g_{\rm X}\frac{M_{\rm d,X}(t)}{M_{\rm X}(t)}\right], \tag{21}$$

where $\rho_{\rm ISM}^{\rm eff}$ is the average mass density of the ISM in which grain growth occurs. As grain growth occurs, the number of gaseous metals decreases. Thus, $n_{\rm X}$ is a decreasing function of time if only grain growth is concerned. The mass density is estimated as $\rho_{\rm ISM}^{\rm eff} = \mu m_{\rm H} n_{\rm H,CNM}$, where μ is the mean atomic weight, assumed to be 1.33 (the mass ratio of hydrogen to helium is $3:1$). In addition, $m_{\rm H}$ and $n_{\rm H,CNM}$ are the mass of a hydrogen atom and the hydrogen number density in the CNM, respectively, and we apply $n_{\rm CNM} = 30\ {\rm cm}^{-3}$. Hence, from the above four equations [Eq. (18)–(21)], we obtain

---

[2] Note that Eq. (17) is valid for the case where only grain growth is considered, i.e., without sputtering, shattering and coagulation.

$$\dot{a} \equiv \frac{\mathrm{d}a}{\mathrm{d}t} = \frac{\alpha \rho_{\mathrm{ISM}}^{\mathrm{eff}}}{g_{\mathrm{X}} s} \frac{M_{\mathrm{X}}(t)}{M_{\mathrm{ISM}}(t)} \left(\frac{kT_{\mathrm{gas}}}{2\pi m_{\mathrm{X}}}\right)^{1/2} \left[1 - g_{\mathrm{X}} \frac{M_{\mathrm{d,X}}(t)}{M_{\mathrm{X}}(t)}\right]. \tag{22}$$

We assume $\alpha = 1$ for simplicity, which means that when the key species collide with a dust grain, it definitely sticks. In our study, we calculate the grain growth using Eqs. (17) and (22).

2.2.5 Shattering

Turbulence occurs in the ISM ubiquitously, and it is confirmed that turbulence is maintained by thermal conduction from simulations (e.g., Koyama & Inutsuka 2002). In a turbulent medium, dust grains are accelerated by turbulence (e.g., McKee & Ostriker 2007), and they collide with each other and shattering can occur (e.g., Yan et al. 2004; Hirashita & Yan 2009; Hirashita et al. 2010). Hirashita & Yan (2009) suggested that the grain size distribution in the ISM changes significantly by shattering due to collisions between dust grains accelerated by magnetohydrodynamic turbulence (Yan et al. 2004). In our model, to calculate shattering process, we adopt the grain velocity calculated by Yan et al. (2004), and the shattering equation and parameters used by Hirashita & Yan (2009), whose formulation is based on Jones, Tielens & Hollenbach (1996).

We outline the treatment of shattering. We define $\rho_{\mathrm{X}}(a,t)\mathrm{d}a = m(a) f_{\mathrm{X}}(a,t)\mathrm{d}a$ as the mass of grains with radii $[a, a+\mathrm{d}a]$ in a unit volume (refer to as “mass density” in this paper). Considering shattering in the collision between two grains with radii a_1 and a_2 (called grains 1 and 2, respectively), the time evolution of $\rho_{\mathrm{X}}(a,t)\mathrm{d}a$ for shattering is expressed as

$$\begin{aligned}\left[\frac{\mathrm{d}\rho_{\mathrm{X}}(a,t)\mathrm{d}a}{\mathrm{d}t}\right]_{\mathrm{shat}} = & - m(a)\rho_{\mathrm{X}}(a,t)\mathrm{d}a \int_{a_{\min}}^{a_{\max}} \alpha[m(a), m(a_1)]\rho_{\mathrm{X}}(a_1,t)\mathrm{d}a_1\mathrm{d}a_1 \\ & + \int_{a_{\min}}^{a_{\max}}\int_{a_{\min}}^{a_{\max}} \alpha[m(a_1), m(a_2)]\rho_{\mathrm{X}}(a_1,t)\mathrm{d}a_1\rho_{\mathrm{X}}(a_2,t)\mathrm{d}a_2 m_{\mathrm{shat}}^{1,2}(a)\mathrm{d}a_1\mathrm{d}a_2, \end{aligned} \tag{23}$$

and

$$\alpha[m(a_1), m(a_2)] = \begin{cases} 0 & (v_{1,2} \leqslant v_{\mathrm{shat}}) \\ \dfrac{\sigma_{1,2} v_{1,2}}{m(a_1)m(a_2)} & (v_{1,2} > v_{\mathrm{shat}}), \end{cases} \tag{24}$$

where $m_{\mathrm{shat}}^{1,2}(a)$ is the total mass of shattered fragments of grain 1 within size bin $[a, a+\mathrm{d}a]$ by a collision between grains 1 and 2, and depends on the relative velocity of the grains. The size distribution of shattered fragments is proportional to $a^{-3.3}$ (e.g., Jones, Tielens & Hollenbach 1996) [3]. The cross section of the collision between grains 1 and 2 is assumed to be $\sigma_{1,2} = \pi(a_1 + a_2)^2]$. The shattering threshold, v_{shat}, is assumed to be $1.2\ \mathrm{km\ s^{-1}}$, and $2.7\ \mathrm{km\ s^{-1}}$ for carbonaceous dust and silicate dust, respectively (Jones, Tielens & Hollenbach 1996). We adopt the same treatment for the relative velocity as Jones et al. (1994) and Hirashita & Yan (2009): Each time step is divided into four small time steps, and we consider shattering under the following four relative velocities in each small time step (i) front collision $(v_{1,2} = v_1 + v_2)$, (ii) back-end collision $(v_{1,2} = |v_1 - v_2|)$, (iii) side collision $v_{1,2} = v_1$, and (iv) $v_{1,2} = v_2$. Here, v_1 and v_2 are the velocities of the grain with radius a_1 and a_2, respectively.

Shattering can occur not only in turbulence but also in SN shocks (e.g., Jones, Tielens & Hollenbach 1996). However, both of these shattering mechanisms have similar consequences on the grain size distribution, so it is difficult to separate them. To compare our work with previous studies (Hirashita et al. 2010; Kuo & Hirashita 2012), we only consider shattering in turbulence.

2.2.6 Coagulation

In low temperature and high density regions of the ISM, it is expected that coagulation by grain–grain collisions occurs. Indeed, Stepnik et al. (2003) observed dense filaments and showed that the ratio of the intensity in the filaments, $I_{60\ \mu\mathrm{m}}/I_{100\ \mu\mathrm{m}}$, is smaller than that in the diffuse ISM. They concluded that this trend resulted from the decrease of small grains due to coagulation. For coagulation, we adopt the formulation, the velocity of grains, and the parameters used by Hirashita & Yan (2009).

The time evolution of $\rho_{\mathrm{X}}(a,t)\mathrm{d}a$ for coagulation is expressed as follows

$$\begin{aligned}\left[\frac{\mathrm{d}\rho_{\mathrm{X}}(a,t)\mathrm{d}a}{\mathrm{d}t}\right]_{\mathrm{coag}} = & - m(a)\rho_{\mathrm{X}}(a,t)\mathrm{d}a \int_{a_{\min}}^{a_{\max}} \alpha[m(a_1), m(a)]\rho_{\mathrm{X}}(a_1,t)\mathrm{d}a_1\mathrm{d}a_1 \\ & + \int_{a_{\min}}^{a_{\max}}\int_{a_{\min}}^{a_{\max}} \alpha[m(a_1), m(a_2)]\rho_{\mathrm{X}}(a_1,t)\mathrm{d}a_1\rho_{\mathrm{X}}(a_2,t)\mathrm{d}a_2 m_{\mathrm{coag}}^{1,2}(a)\mathrm{d}a_1\mathrm{d}a_2, \end{aligned} \tag{25}$$

and

$$\alpha[m(a_1), m(a_2)] = \begin{cases} 0 & (v_{1,2} \geqslant v_{\mathrm{coag}}^{1,2}) \\ \dfrac{\beta\sigma_{1,2} v_{1,2}}{m(a_1)m(a_2)} & (v_{1,2} < v_{\mathrm{coag}}^{1,2}), \end{cases} \tag{26}$$

---

[3] The method of calculation of the maximum and minimum size of fragments is described in detail in Section 2.3 in Hirashita & Yan (2009).

where β is the sticking coefficient of dust grains, and $m^{1,2}_{\rm coag}(a) = m(a_1)$ if the mass range of $m(a_1) + m(a_2)$ is within $[m(a), m(a) + {\rm d}m(a)]$; otherwise $m^{1,2}_{\rm coag}(a) = 0$.

We assume that coagulation occurs if the relative velocity is less than the coagulation threshold $v^{1,2}_{\rm coag}$. In our model, it is calculated in the same way as Hirashita & Yan (2009),

$$v^{1,2}_{\rm coag} = 21.4 \left[\frac{a_1^3 + a_2^3}{(a_1 + a_2)^3} \right]^{1/2} \frac{\gamma^{5/6}}{E^{1/3} R_{1,2}^{5/6} s^{1/2}}, \tag{27}$$

where $R_{1,2} \equiv a_1 a_2/(a_1 + a_2)$, γ is the surface energy per unit area, and $1/E = [(1-\nu_1)^2/E_1 + (1-\nu_2)^2/E_2]$, where ν_1 and E_1 are Poisson's ratio and Young's modulus of grain 1. The parameters we used are shown in Table 1. Here, we assume $\beta = 1$ for simplicity. The treatment of the relative velocity is the same as for shattering.

2.2.7 *Formulation of the grain-size dependent evolution of dust mass*

Here, using the dust processes introduced above, we show the equation for the dust mass evolution in a galaxy at each grain radius bin, so that we can finally obtain the evolution of grain size distribution. Defining $\Delta M_{\rm d}(a,t) \equiv m(a) f(a,t) \Delta a$ as the mass density of grains with radii $[a, a + \Delta a]$ [4] and a galactic age t, it is formulated as

$$\begin{aligned}
\frac{{\rm d}\Delta M_{\rm d}(a,t)}{{\rm d}t} &= -\frac{\Delta M_{\rm d}(a,t)}{M_{\rm ISM}(t)} + \Delta Y_{\rm d}(a,t) \\
&\quad - \frac{M_{\rm swept}}{M_{\rm ISM}(t)} \gamma_{\rm SN}(t) \left[\Delta M_{\rm d}(a,t) - m(a) \int_0^\infty \xi(a,a^{'}) \Delta a f(a^{'},t) {\rm d}a' \right] \\
&\quad + \eta_{\rm CNM} \left[m(a) \Delta a \frac{\partial [f(a,t)]}{\partial t} \right] \\
&\quad + \eta_{\rm WNM} \left[\frac{{\rm d}\Delta M_{\rm d}(a,t)}{{\rm d}t} \right]_{\rm shat,WNM} + \eta_{\rm CNM} \left[\frac{{\rm d}\Delta M_{\rm d}(a,t)}{{\rm d}t} \right]_{\rm shat,CNM} \\
&\quad + \eta_{\rm WNM} \left[\frac{{\rm d}\Delta M_{\rm d}(a,t)}{{\rm d}t} \right]_{\rm coag,WNM} + \eta_{\rm CNM} \left[\frac{{\rm d}\Delta M_{\rm d}(a,t)}{{\rm d}t} \right]_{\rm coag,CNM},
\end{aligned} \tag{28}$$

where $\eta_{\rm WNM}$ and $\eta_{\rm CNM}$ are the mass fraction of WNM and CNM in the ISM, respectively. From top to bottom, the terms on the right hand side describe reduction of dust due to astration, ejection of dust from stellar sources, dust destruction by SN shocks, grain growth in the CNM, shattering in the WNM and CNM, and coagulation in the WNM and CNM. To calculate the dust processes which occur in each ISM phase, as mentioned in Section 1, we assume (1) that $\eta_{\rm WNM}$ and $\eta_{\rm CNM}$ are constants and (2) that there are two stable phases, WNM and CNM, in the ISM (namely, the sum of $\eta_{\rm WNM}$ and $\eta_{\rm CNM}$ is unity).

The total mass of grains with radii $[a, a + \Delta a]$ ejected by stars per unit time, $\Delta Y_{\rm d}(a,t)$, is expressed as

$$\Delta Y_{\rm d}(a,t) = \int_{m_{\rm cut}(t)}^{100\ {\rm M}_\odot} \Delta m_{\rm d}(m, Z(t-\tau_m), a) \phi(m) {\rm SFR}(t-\tau_m) {\rm d}m, \tag{29}$$

where $\Delta m_{\rm d}(m, Z, a)$ is the total mass of grains with radii $[a, a + \Delta a]$ released by stars with mass m and metallicity Z.

3 MODEL RESULTS

In this paper, as mentioned above, we consider the effects of dust formation by SNe II and AGB stars, dust destruction by SN shocks in the ISM, grain growth, shattering, and coagulation on the evolution of grain size distribution in galaxies. Among these processes, dust formation by SNe II and AGB stars, dust destruction and grain growth directly increase or decrease the total dust mass, while shattering and coagulation modify only the grain size distribution. The evolution of the total dust mass in galaxies is often modeled by taking into account the former four contributions (dust formation by SNe II and AGB stars, dust destruction, and grain growth) (e.g., Dwek & Scalo 1980; Dwek 1998; Calura, Pipino & Matteucci 2008; Zhukovska, Gail, & Trieloff 2008; Pipino et al. 2011; Inoue 2011; Asano et al. 2013). They calculated the dust evolution by assuming a representative grain size, but the dust destruction and grain growth depend on the grain size distribution. Thus, it is unknown whether these four contributions can reproduce the grain size distribution in nearby galaxies even though they can explain the evolution of the total dust mass. In Section 3.1, we first investigate the contributions of the processes that directly affect the total dust mass, and then in Section 3.2, we examine the effects of shattering and coagulation.

---

[4] In this Section, we use the symbol "Δ" to emphasize that it stands not for infinitesimal but a certain small amount.

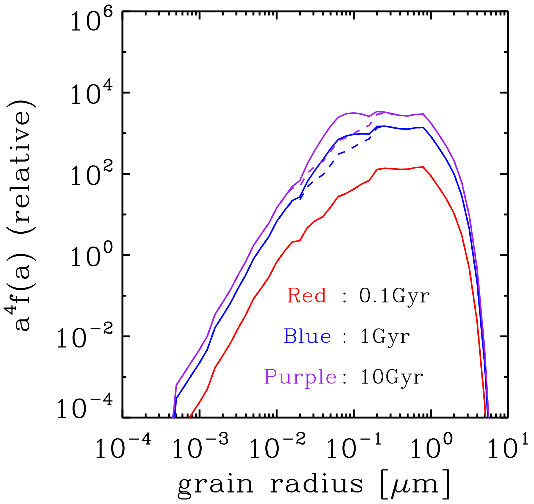

Figure 1. Grain size distribution taking into account the dust production by AGB stars and SNe II and dust reduction through astration (solid lines). Red, blue, and purple lines represent the cases at $t = 0.1, 1.0$, and 10 Gyr, respectively, with $\tau_{\rm SF} = 5$ Gyr and $n_{\rm SN} = 1.0$ cm^{-3}. Dashed lines are cases with dust production by SNe II only and dust reduction through astration, the same color corresponding to the same age. Note that the red dashed line overlaps with the red solid line.

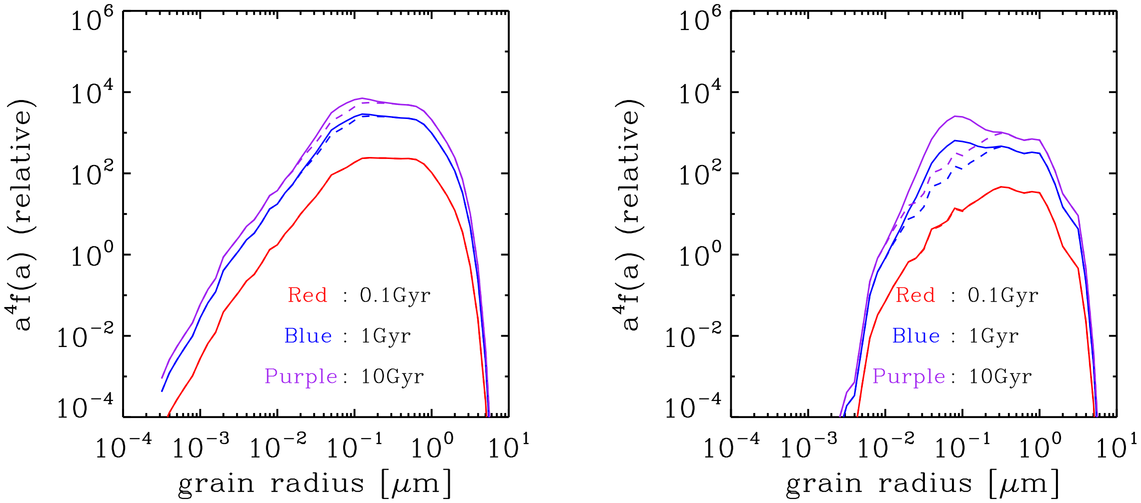

Figure 2. Same as in Fig. 1, but we adopt different values of $n_{\rm SN}$: 0.1 cm^{-3} in the left panel and 10.0 cm^{-3} in the right panel. Note that the red dashed lines overlap with the red solid lines.

3.1 Without the effects of grain–grain collisions

3.1.1 Stellar processes

First, we consider the stellar processes including dust ejection from stars (SNe II and AGB stars) and dust reduction via astration. Figure 1 shows the result. The size distribution is expressed by multiplying a^4 to show the mass distribution in logarithmic grain radius bin. We adopt $\tau_{\rm SF} = 5$ Gyr and $n_{\rm SN} = 1.0$ cm^{-3}. We also show the cases with SNe II only. As mentioned in Section 2, since $M_{\rm tot}$ is just a scale factor, the shape of the size distribution does not change with $M_{\rm tot}$. From Fig. 1, throughout any galactic age, we can observe that the grain size distribution has a peak at around 0.5 μm, and that only a small amount of grains with $a < 0.01$ μm can be formed by stars. In Fig. 2, we show the grain size distribution for other values of $n_{\rm SN}$: 0.1 cm^{-3} in the left panel and 10.0 cm^{-3} in the right panel, respectively. From Figure 2, we find that a larger amount of dust grains with radii less than ~ 0.1 μm are destroyed by reverse shocks in the case of higher $n_{\rm SN}$, and a smaller amount of dust is supplied to the ISM. However, even if $n_{\rm SN}$ changes, the trend that a small amount of dust grains with radii less than 0.01 μm are supplied to the ISM does not change. Thus, stars are the sources of dust grains with large radii ($\geqslant 0.05$ μm).

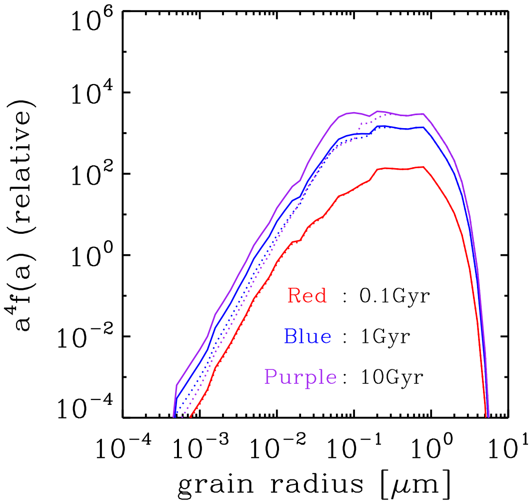

Figure 3. Grain size distribution taking into account the dust destruction by SN shocks in the ISM in addition to the processes in Fig. 1 (dotted lines). The values of $\tau_{\rm SF}$ and $n_{\rm SN}$ are the same as in Fig. 1. Solid lines are the same as in Fig. 1, the same color corresponding to the same age. Note that the red dotted line overlaps with the red solid line.

From Figs. 1 and 2, we observe that dust from SNe II always dominates the grain size distribution, while the contribution of dust from AGB stars is seen only around $0.1\ \mu$m at a galactic age $t = 10$ Gyr. From our calculation, for the case with $n_{\rm SN} = 1.0\ {\rm cm}^{-3}$, the dust mass ratios produced by AGB stars and SNe II are 1.6×10^{-3}, 0.16, and 0.37 at $t = 0.1, 1.0$ and 10 Gyr, respectively. On the other hand, Valiante et al. (2009) suggested that the contribution of AGB stars to the total dust mass in galaxies approaches or exceeds that of SNe II at $t \sim 1$ Gyr. This difference mainly results from the dust mass data adopted. We adopt the data of Nozawa et al. (2007), whereas Valiante et al. (2009) adopted those of Bianchi & Schneider (2007). The dust mass of Nozawa et al. (2007) is larger than that of Bianchi & Schneider (2007) because of the difference in the treatment of the dust condensation and the destruction by reverse shocks. However, even if the contribution of AGB stars is larger, the result that only a small amount of grains with $\lesssim 0.01\ \mu$m are produced by stars does not change.

From the right panel in Fig. 2, we find that the contribution of dust from AGB stars is relatively large for $n_{\rm SN} = 10.0\ {\rm cm}^{-3}$ at $t = 10$ Gyr. At $t = 10$ Gyr, the dust mass ratios produced by AGB stars and SNe II are 0.16, 0.37, and 1.39 for the cases with $n_{\rm SN} = 0.1, 1.0$ and $10.0\ {\rm cm}^{-3}$, respectively. This is because a larger amount of dust grains condensed in the ejecta of SNe II are destroyed by reverse shocks for higher $n_{\rm SN}$.

3.1.2 Dust destruction by SN shocks in the ISM

In Fig. 3, we show the evolution of the grain size distribution taking into account dust destruction by SN shocks in the ISM in addition to the dust production by SNe II and AGB stars. We also present the cases without the dust destruction (i.e., the same as the solid lines of Fig. 1). The values of $\tau_{\rm SF}$ and $n_{\rm SN}$ are set to the same values as in Fig. 1. At $t \lesssim 1.0$ Gyr, the grain size distributions with and without the dust destruction by SN shocks in the ISM are very similar to each other.

Now we estimate the dust destruction timescale. First, we introduce the sweeping timescale, $\tau_{\rm sweep}$, at which SN shocks sweep the whole ISM, as

$$\tau_{\rm sweep} \equiv \frac{M_{\rm ISM}}{M_{\rm swept}\gamma_{\rm SN}}. \tag{30}$$

From Eq. (15), if C is defined as

$$C \equiv \int_{8\ {\rm M}_\odot}^{40\ {\rm M}_\odot} \phi(m){\rm d}m, \tag{31}$$

Eq. (15), with Eq. (4), can be approximated as

$$\gamma_{\rm SN} \simeq C\frac{M_{\rm ISM}}{\tau_{\rm SF}}, \tag{32}$$

where C is about 1.5×10^{-2} from our calculation. Thus, if $n_{\rm SN} = 1.0\ {\rm cm}^{-3}$, $\tau_{\rm sweep} \sim$ 2–4 $\times 10^{-2}\tau_{\rm SF}$. Next, we approximate the dust destruction rate by introducing the dust destruction timescale, $\tau_{\rm SN}$, as

$$\left.\frac{{\rm d}M_{\rm d}}{{\rm d}t}\right|_{\rm SN} \sim -\frac{M_{\rm d}}{\tau_{\rm SN}}. \tag{33}$$

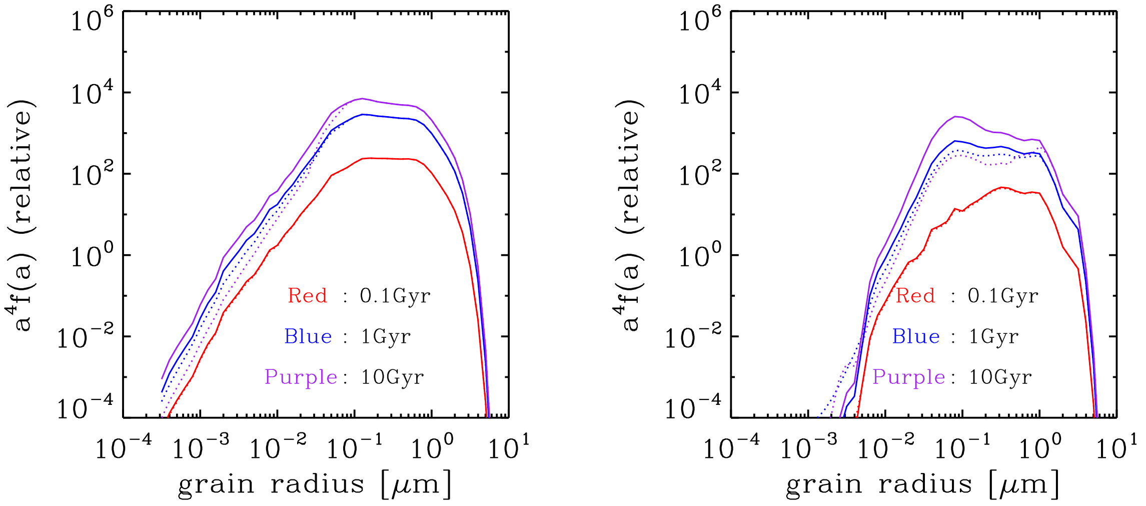

Figure 4. Same as in Fig. 3, but we adopt different values of $n_{\rm SN}$: $0.1\ {\rm cm}^{-3}$ in the left panel and $10.0\ {\rm cm}^{-3}$ in the right panel. Note that the red dotted lines overlap with the red solid lines.

The right hand side of Eq. (14) can be approximated as $-\tau_{\rm sweep}^{-1}M_{\rm d}(1-\xi)$ where ξ is a typical value of $\xi_{\rm X}(a,a^{'})$; then, Eq. (14) reduces to

$$\tau_{\rm SN} \sim (1-\xi)^{-1}\tau_{\rm sweep}. \tag{34}$$

Since the overall efficiency of dust destruction, $(1-\xi)$, is ~ 0.3 for $n_{\rm SN} = 1.0\ {\rm cm}^{-3}$ (Nozawa et al. 2006), we obtain $\tau_{\rm SN} \sim 0.1\tau_{\rm SF}$. Thus, the difference between the cases with and without dust destruction cannot be seen at $t = 0.1$ Gyr in Fig. 3, where $\tau_{\rm SN} \sim 0.1\tau_{\rm SF} \sim 0.5$ Gyr.

We find that dust grains with $a \lesssim 0.1\ \mu$m are destroyed effectively at 10 Gyr $\gg \tau_{\rm SN}$ (compare the solid and dotted lines in Fig. 3). Since the decreasing rate of grain radius by sputtering does not depends on the grain radius, smaller grains are effectively destroyed in SN shocks, and the amount of smaller grains decreases (Nozawa et al. 2006).

In Fig. 4, we show the cases with $n_{\rm SN} = 0.1$ and $10\ {\rm cm}^{-3}$. Comparing figs. 3 and 4, we find that a larger amount of dust grains are destroyed for higher $n_{\rm SN}$. The destruction effect is more pronounced at small sizes. Indeed, we observe that grains with $a \lesssim 1.0\ \mu$m are effectively destroyed in the case with $n_{\rm SN} = 10.0\ {\rm cm}^{-3}$. Nevertheless, the result that smaller grains are effectively destroyed does not change, and we find that dust grains with radii larger than $0.1\ \mu$m mainly dominate the total dust amount in galaxies. Consequently, if the dust destruction by sputtering in SN shocks is dominant, only large ($a \gtrsim 0.1\ \mu$m) grains can survive in the ISM.

3.1.3 Grain growth

Figure 5 shows the evolution of the grain size distribution taking into account the dust production from stellar sources, dust destruction, and grain growth. We adopt $\tau_{\rm SF} = 5$ Gyr, $n_{\rm SN} = 1.0\ {\rm cm}^{-3}$, and the mass fraction for the CNM, $\eta_{\rm CNM} = 0.5$. From Fig. 5, we observe that while the grain size distributions with and without grain growth are almost the same at ages 0.1 Gyr and 1 Gyr, the difference is clear at 10 Gyr. The effect of grain growth is prominent around $a \sim 0.3\ \mu$m at 10 Gyr, since the total surface area of grains is dominated by grains with $a \sim 0.3\ \mu$m. The timescale of grain growth is discussed in detail in Section 4.

In Fig. 5, we also plot the slope of the MRN size distribution, $f(a){\rm d}a \propto a^{-3.5}{\rm d}a$ (Mathis, Rumpl & Nordsieck 1977), which is thought to be the grain size distribution in the Milky Way. From Fig. 5, it is clear that the small grains with $a \lesssim 0.01\ \mu$m are too few to reproduce the MRN size distribution. However, the existence of the 70 μm excess is considered to be a proof of the existence of small grains (Bernard et al. 2008). Furthermore, Takeuchi et al. (2003, 2005) argued by using their infrared SED model that small grains are necessary to reproduce the near–mid infrared SEDs of star forming galaxies. Consequently, when we consider the case in which dust production by SNe II and AGB stars, dust destruction, and grain growth take place, the grain size distribution is always dominated by large grains, and we need to consider other processes to produce small grains efficiently.

3.2 Grain–grain collision effects

In the above we have investigated the dust processes which directly affect the evolution of the total dust mass in galaxies: dust production by AGB stars and SNe II, dust destruction by SN shocks, and grain growth. As shown above, these processes cannot produce small grains ($a \lesssim 0.01\ \mu$m) efficiently. Therefore, we now consider the contributions of the grain–grain collisions, shattering and coagulation in turbulence, to the grain size distribution. If these processes occur, although the total dust mass in galaxies does not change, the grain size distribution does.

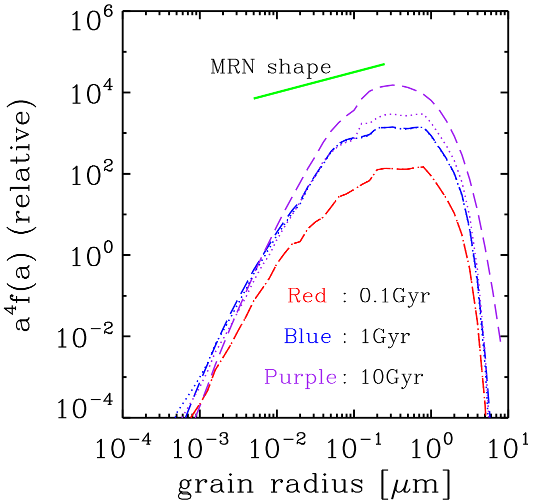

Figure 5. Grain size distribution taking into account the dust production from stellar sources, dust destruction, and grain growth with $\tau_{\rm SF} = 5$ Gyr and $n_{\rm SN} = 1.0\ {\rm cm}^{-3}$ (long-dashed lines). We adopt $\eta_{\rm CNM} = 0.5$. Dotted lines represent cases without grain growth [the same as in Fig. (3)], the same color corresponding to the same age. Note that the red dotted line overlaps with the red long-dashed line. Green solid line represents the slope of the power-law grain size distribution with index -3.5 [$f(a){\rm d}a \propto a^{-3.5}{\rm d}a$ (Mathis, Rumpl & Nordsieck 1977)] which is thought to be the grain size distribution in the Milky Way.

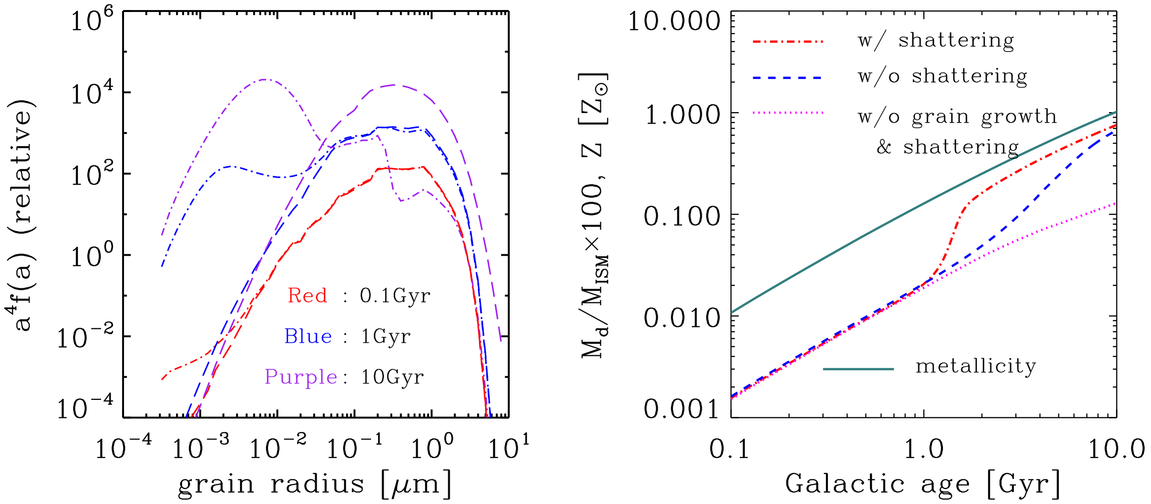

Figure 6. Left panel: grain size distribution with (dot-dashed lines) and without (long-dashed lines) shattering (all other dust processes in Section 3.1 are included). Note that the red dot-dashed line overlaps with the red long-dashed line. Right panel: time evolution of dust-to-gas mass ratio with (solid line) and without (dotted line) shattering. The case without grain growth and shattering (dashed line) is also plotted. Dot-dashed line represents the evolution of metallicity. The parameters $\tau_{\rm SF}$ and $n_{\rm SN}$ are set to be 5 Gyr and $1.0\ {\rm cm}^{-3}$, respectively. We adopt $\eta_{\rm WNM} = \eta_{\rm CNM} = 0.5$.

3.2.1 Shattering

In the left panel of Fig. 6, we show the evolution of the grain size distribution in the galaxy with and without shattering (all other dust processes in Section 3.1 are included). The right panel of Fig. 6 shows the time evolution of dust-to-gas mass ratio ($M_{\rm d}/M_{\rm ISM}$) for the cases with and without shattering, respectively. We also plot the case without grain growth and shattering and the evolution of metallicity in the same panel. The parameters $\tau_{\rm SF}$ and $n_{\rm SN}$ are set to be 5 Gyr and $1.0\ {\rm cm}^{-3}$, respectively. We adopt $\eta_{\rm WNM} = \eta_{\rm CNM} = 0.5$.

From the left panel of Fig. 6, at the early stage of galaxy evolution (0.1 Gyr) the size distributions with and without shattering are similar with only a little difference at small sizes. At 1 Gyr, we observe that the size distribution has a bump at $a \sim 0.001$ μm in the case with shattering. As time passes, the amount of large grains decreases, and as a result the size distribution is dominated by small grains. This behavior is substantially different from that of the case without shattering. We now discuss this behavior in more detail.

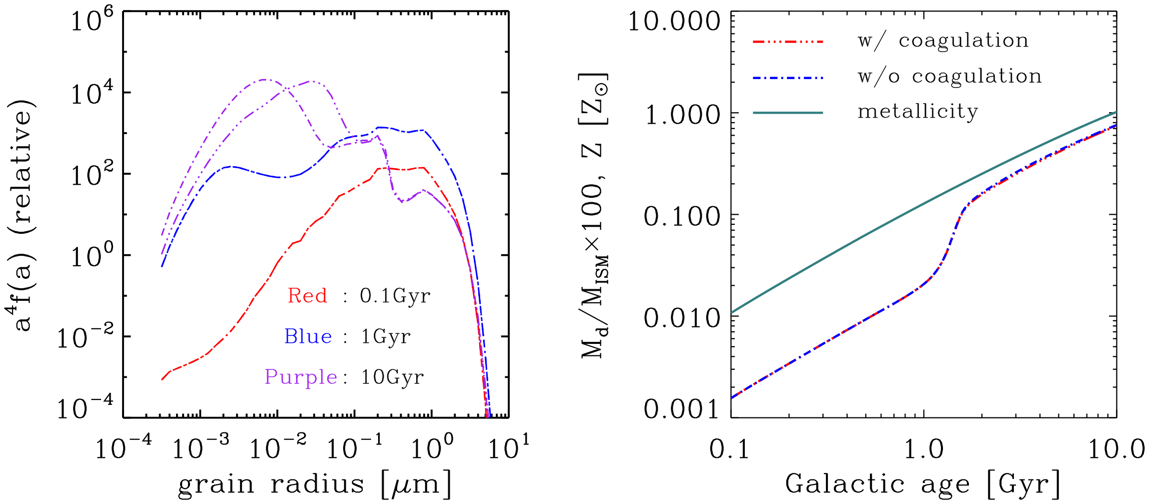

Figure 7. Left panel: grain size distribution with (triple-dot-dashed lines) and without (dot-dashed lines) coagulation (all the other dust processes are included). Note that the red and blue dot-dashed lines overlap with the red and blue triple-dot-dashed lines. Right panel: time evolution of dust-to-gas mass ratio with (solid line) and without (dotted line) coagulation. Dot-dashed line represents the evolution of metallicity. The values of parameters ($\tau_{\rm SF}, n_{\rm SN}, \eta_{\rm WNM}$, and $\eta_{\rm CNM}$) are the same as in Fig. 6.

As shown in Eq. (23), the efficiency of shattering is larger for larger amount of grains (Hirashita 2010). At 0.1 Gyr, the efficiency of shattering is low because of the small dust abundance. As a result, there is only a small difference between the cases with and without shattering. At $t = 1$ Gyr, since shattering occurs efficiently due to the increased amount of large grains, the amount of small grains increases. At the same time, we observe that the grain size distribution has little difference between the cases with and without shattering at $a > 0.1$ μm in the left panel of Fig. 6. This is because shattering of a tiny fraction of large grains can produce a large amount of small grains (Hirashita et al. 2010). Furthermore, since the number of small grains increases, the small grains dominate the total grain surface area. Consequently, grain growth occurs at the smallest grain sizes ($a \lesssim 10^{-3}$ μm), forming a bump at $\sim 10^{-3}$–10^{-2} μm. At $t = 10$ Gyr, since the number of small grains increases, large grains are shattered more efficiently by the frequent collisions with the small grains. Consequently, comparing the grain size distribution at 10 Gyr with that at 1 Gyr, the amount of large grains decreases significantly. Furthermore, because of grain growth, the bump is shifted to a larger size at 10 Gyr than at 1 Gyr, and finally the size distribution has a large bump at $a \sim 0.01$ μm at 10 Gyr.

Focusing on the grain size distribution at 10 Gyr, we find that if shattering occurs, the amount of grains with $a > 0.2$ μm is more than two orders of magnitude smaller than that of grains with $a < 0.2$ μm. Thus, the maximum size of grains in diffuse ISM is determined not by stardust but by the process of shattering.

In the right panel of Fig. 6, we find that grain growth starts to increase the total dust mass at around $t = 1$ Gyr as seen in the rapid increase of dust-to-gas mass ratio, and grain growth becomes more rapid in the case with shattering than in the case without shattering because of the increased number of small grains. As discussed in Kuo & Hirashita (2012), shattering contributes not only to the evolution of the grain size distribution but also to the total dust mass in galaxies indirectly through the enhanced grain growth. Thus, shattering is a very important process in understanding the evolution of the size distribution and the amount of dust grains in the ISM.

3.2.2 Coagulation

In Fig. 7, we show the evolution of the grain size distribution with and without coagulation (all the other dust processes are included) in the left panel, and the time evolutions of dust-to-gas mass ratio with and without coagulation and of metallicity in the right panel. The parameters adopted are the same as in Fig. 6.

From the left panel of Fig. 7, we find that there is little difference between the cases with and without coagulation at 0.1 and 1.0 Gyr. Since larger grains are coupled with the larger-scale turbulence, they can obtain larger velocity dispersions. Thus, coagulation mainly occurs by collisions between small grains whose velocity dispersions are smaller than the coagulation threshold [Eq. (27)]. However, since the abundance of small grains is low, the contribution of coagulation is not seen at 0.1 and 1 Gyr before shattering becomes effective. After that, a large abundance of small grains are produced by shattering so coagulation becomes effective. Consequently, the bump at $a \sim 0.01$ μm shifts to a larger size by coagulation.

From the right panel of Fig. 7, we find that the evolution of the total dust mass does not change significantly by coagulation, confirming the result obtained by Hirashita (2012). If coagulation occurs, the number of small grains decreases; as a result, the surface-to-volume ratio

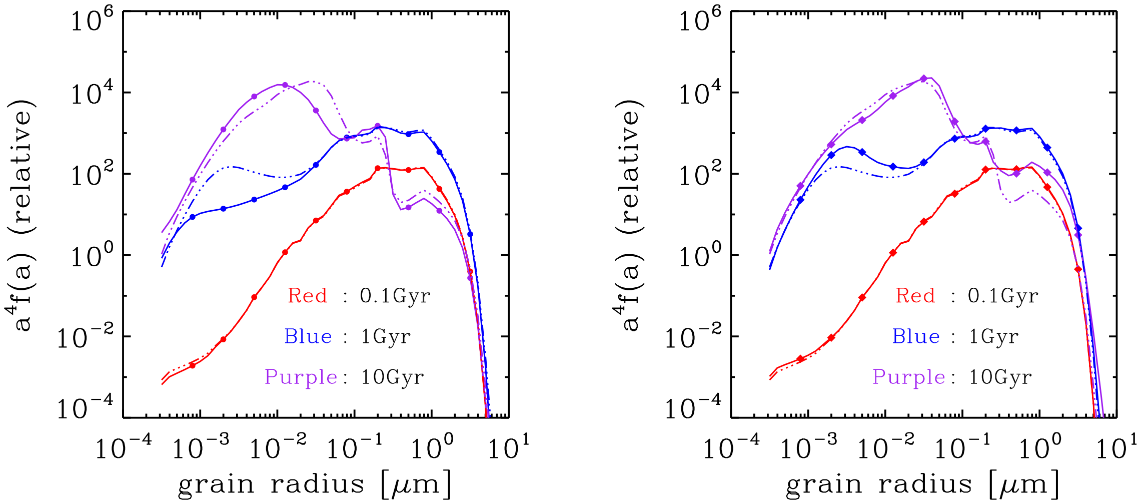

Figure 8. Grain size distribution with $(\eta_{\rm WNM}, \eta_{\rm CNM}) = (0.9, 0.1)$ (solid lines with filled circles in the left panel) and $(0.1, 0.9)$ (solid lines with filled diamonds in the right panel). The values of parameters $\tau_{\rm SF}$ and $n_{\rm SN}$ are the same as in Fig. 7. Triple-dot-dashed lines are the case with $\eta_{\rm WNM} = \eta_{\rm CNM} = 0.5$.

of grains decreases. This effect may suppress the increase in dust mass due to grain growth. However, since grain growth becomes inefficient to the dust evolution before coagulation becomes efficient (the details are shown in Section 4), the contribution of coagulation cannot be observed for the total dust mass evolution. Consequently, the effect of coagulation on the evolution of the total dust mass in galaxies is negligible.

From the left panel of Fig. 7, we find that the amount of grains with $a > 0.2$ μm does not change significantly by coagulation because coagulation cannot occur by collision between large grains which have larger velocity dispersions than the coagulation threshold. Thus, although the bump of the grain size distribution is shifted to a larger size by coagulation, coagulation does not affect the maximum size determined by shattering (Section 3.2.1).

3.3 Parameter dependence

Shattering and coagulation occur differently in both ISM phases (WNM and CNM). Here, by adopting $(\eta_{\rm WNM}, \eta_{\rm CNM}) = (0.9, 0.1)$ and $(0.1, 0.9)$, we show the effect of ISM phases.

In Fig. 8, we show the evolution of the grain size distribution with $(\eta_{\rm WNM}, \eta_{\rm CNM}) = (0.9, 0.1)$ (left panel) and $(0.1, 0.9)$ (right panel). The case with $\eta_{\rm WNM} = \eta_{\rm CNM} = 0.5$ is shown for comparison. At $t = 0.1$ Gyr, the grain size distributions are almost the same in all the cases, since the dust process is dominated by the production by stellar sources. At $t = 1$ Gyr, the amount of dust grains with $a < 0.01$ μm is larger for the case with larger $\eta_{\rm CNM}$ because grain growth is more efficient. At 10 Gyr, the difference is clear at each grain size. For larger $\eta_{\rm WNM}$, the decrements of the amount of dust grains with $a > 0.2$ μm is larger because shattering in the WNM is more efficient. Furthermore, for larger $\eta_{\rm CNM}$, the bump produced by grain growth around 0.01 μm shifts to a larger size. Thus, we understand that the amount of dust grains with $a > 0.2$ μm and the shift of the bump around 0.01 μm are dominated by shattering in WNM and coagulation in CNM, respectively. In addition, comparing the two panels in Fig. 8, we find that the dust amount at $a \sim 0.1$–0.2 μm tends to be smaller for a larger $\eta_{\rm CNM}$ [5]. It means that the amount of dust grains with $a \sim 0.1$ μm is dominated not by shattering in WNM but shattering in CNM. Hence, the grain size distribution in galaxies is finally dominated by processes in WNM for large grains (> 0.2 μm) and by processes in CNM for small grains (~ 0.1 μm).

4 DISCUSSION

In Section 3, we showed the evolution of the grain size distribution in galaxies for a variety of mixture of dust processes. We found that the grain size distribution is dominated by large grains produced by stars (SNe II and AGB stars) in the early stage of galaxy evolution, but as the time passes the number of small grains increases due to shattering, and the small grains grow to larger grains by grain growth. After that, the size distribution shifts to larger sizes due to coagulation. Thus, we conclude that, while the grain size distribution in galaxies is controlled by stellar processes in the early stage of galaxy evolution, the main driver to change the size distribution is replaced with the processes in the ISM (shattering, coagulation, and grain growth) at the later stage of galaxy evolution. These processes (shattering, coagulation, and grain growth) have timescales dependent on the grain size distribution. In this Section, by adopting representative grain radii, 0.001 μm, 0.01 μm, 0.1 μm, and 1.0 μm, we discuss the evolution of the grain size distribution more quantitatively.

---

[5] The mass ratio of grains with $a \sim 0.1$–0.2 μm for the cases between $(\eta_{\rm WNM}, \eta_{\rm CNM}) = (0.5, 0.5)$ and $(0.9, 0.1)$ is about 0.6 at $t = 10$ Gyr.

Figure 9 shows the time evolution of the ratio between the size distribution functions, $f(a)$, and $f(a)_{\rm star}$, the latter being obtained by considering only the stellar processes [the first and second terms in the right hand size of Eq. (28)]. Panels (a), (b), and (c) are the cases with $(\eta_{\rm WNM}, \eta_{\rm CNM}) = (0.5, 0.5), (0.9, 0.1)$, and $(0.1, 0.9)$, respectively, for $\tau_{\rm SF} = 5$ Gyr and $n_{\rm SN} = 1.0\ {\rm cm}^{-3}$. From Fig. 9, we find that behavior of $f(a)/f(a)_{\rm star}$ depends strongly on the grain radius. As mentioned above, this is because each dust process works at different grain radii on different timescales. First, we discuss the evolution of the grain size in panel (a). We find that $f(a)/f(a)_{\rm star}$ at $a = 0.001$ μm starts to deviate from unity at the earliest galactic age among all four grain sizes. The process that causes this increase is shattering. These small grains are produced by shattering between large grains produced by stars. Furthermore, as mentioned in Section 3.2.1, since shattering of a small number of large grains can produce a large number of small grains, we cannot see the change of $f(a)/f(a)_{\rm star}$ for $a = 0.1$ and 1.0 μm.

At $t \sim$ a few hundreds of Myr, $f(a)/f(a)_{\rm star}$ at $a = 0.01$ μm increases. This increase is also due to shattering. The reason why the effect of shattering appears at $a = 0.01$ μm later than at $a = 0.001$ μm is that the size distribution of shattered fragments is proportional to $a^{-3.3}$ (see Section 2.2.5). In other words, the shattered fragments become dominant at smaller sizes on shorter timescales than at larger sizes.

At $t \sim 1$ Gyr, we find that the increase of $f(a)/f(a)_{\rm star}$ at $a = 0.01$ μm is accelerated. This indicates that another process becomes efficient, and it is grain growth. As seen from Fig. 6, as grain growth becomes efficient around 1 Gyr, the amount of grains with less than $a \sim 0.01$ μm increases significantly.

At $t \sim 2$ Gyr, we find that $f(a)/f(a)_{\rm star}$ decrease at all sizes. These decreases are due to coagulation for small grains ($a = 0.001$ and 0.01 μm) and shattering for large grains ($a = 0.1$ and 1.0 μm). As we showed in Section 3.2.2, coagulation mainly occurs between small grains. Thus, the coagulation effect cannot be seen at early phase of galaxy evolution when the abundance of small ($a \lesssim 0.01$ μm) grains is small. Shattering can also occur effectively if there is a large amount of small grains because of a high grain–grain collision rate with small grains [cf. Eq. (24)]. In addition, the main reason why the decrements of grains with $a = 0.1$ and 1.0 μm are different is shattering in different ISM phases. As shown in Section 3.3, grains with $a > 0.2$ μm are mainly dominated by shattering in WNM, while grains with $a \sim 0.1$ μm are dominated by shattering in CNM. In summary, at early phase of galaxy evolution ($t \lesssim 10$ Myr), the size distribution is dominated by dust grains produced by stars, after $t \gtrsim 100$ Myr, the dust processes in the ISM begin to affect the size distribution at small size, and at $t \sim 2$ Gyr (for $\tau_{\rm SF} = 5$ Gyr), various dust processes in the ISM affect all sizes of grains.

Panels (b) and (c) in Fig. 9 show the cases with $(\eta_{\rm WNM}, \eta_{\rm CNM}) = (0.9, 0.1)$ and (0.1, 0.9), respectively. Compared with panel (a), we find that $f(a)/f(a)_{\rm star}$ at $a = 0.01$ μm does not decrease at 10 Gyr in panel (b). This is because the timescale of coagulation becomes longer for smaller $\eta_{\rm CNM}$. From panel (c) ($\eta_{\rm WNM} = 0.1, \eta_{\rm CNM} = 0.9$), we find that the decrement at $a = 1.0$ μm is smaller than those in the cases of panel (a) and (b). This is because the efficiency of shattering in WNM is smaller for smaller $\eta_{\rm WNM}$. However, from all the three panels, we can observe that the timing at which $f(a)/f(a)_{\rm star}$ at all sizes changes due to the dust processes in the ISM (in this case, it is about 2 Gyr) does not vary significantly by the change of ($\eta_{\rm WNM}, \eta_{\rm CNM}$) for the same star formation timescale.

In order to discuss the effect of $\tau_{\rm SF}$ on the size distribution, the results are shown for the same values of the parameters as in the panel (a) of Fig. 9, but for $\tau_{\rm SF} = 0.5$ Gyr in panel (d) and $\tau_{\rm SF} = 50$ Gyr in panel (e). Compared with panel (a), we find that $f(a)/f(a)_{\rm star}$ change at earlier stages for shorter $\tau_{\rm SF}$ at all sizes. This is explained as follows. If $\tau_{\rm SF}$ is short, the amounts of dust and metals released by stars are large at early phases of galaxy evolution. The timescales of shattering and coagulation are inversely proportional to the dust-to-gas mass ratio (e.g., Hirashita 2010; Hirashita & Omukai 2009), and the timescale of grain growth is inversely proportional to metallicity (e.g., Asano et al. 2013). Thus, for shorter $\tau_{\rm SF}$, dust processes in the ISM (grain growth, shattering, and coagulation) begin to affect the size distribution at earlier stages of galaxy evolution ($\sim$ 0.6, 2 and 5 Gyr for $\tau_{\rm SF} = 0.5, 5$, and 50 Gyr, respectively). The timescale of the change of $f(a)/f(a)_{\rm star}$ is roughly estimated to be ~ 1 ($\tau_{\rm SF}$/Gyr)$^{1/2}$ Gyr (Appendix B). We conclude that the grain size distribution in galaxies changes drastically through the galaxy evolution because different dust processes operate on the grain size distribution at different ages.

5 CONCLUSIONS

We constructed a dust evolution model taking into account the grain size distribution in a galaxy, and investigated what kind of dust processes dominate the grain size distribution at each stage of galaxy evolution. In this paper, we considered dust formation by SNe II and AGB stars, dust destruction by SN shocks in the ISM, grain growth in the CNM, and grain–grain collisions (shattering and coagulation) in the WNM and CNM.

We found that the grain size distribution in galaxies is dominated by large grains produced by stars in the early stage of galaxy evolution, but as time passes the size distribution is controlled by processes in the ISM (grain growth, shattering, and coagulation) and the age at which these ISM processes enter depends on the star formation timescale, as $\sim 1(\tau_{\rm SF}/{\rm Gyr})^{1/2}$ Gyr. While dust production by SNe II and AGB stars, dust destruction by SN shocks, and grain growth in the CNM directly affect the total dust mass evolution, we found that the grains are predominantly large ($a \sim$ 0.2–0.5 μm) and only a small amount of small grains ($a < 0.01$ μm) are produced by these processes. If

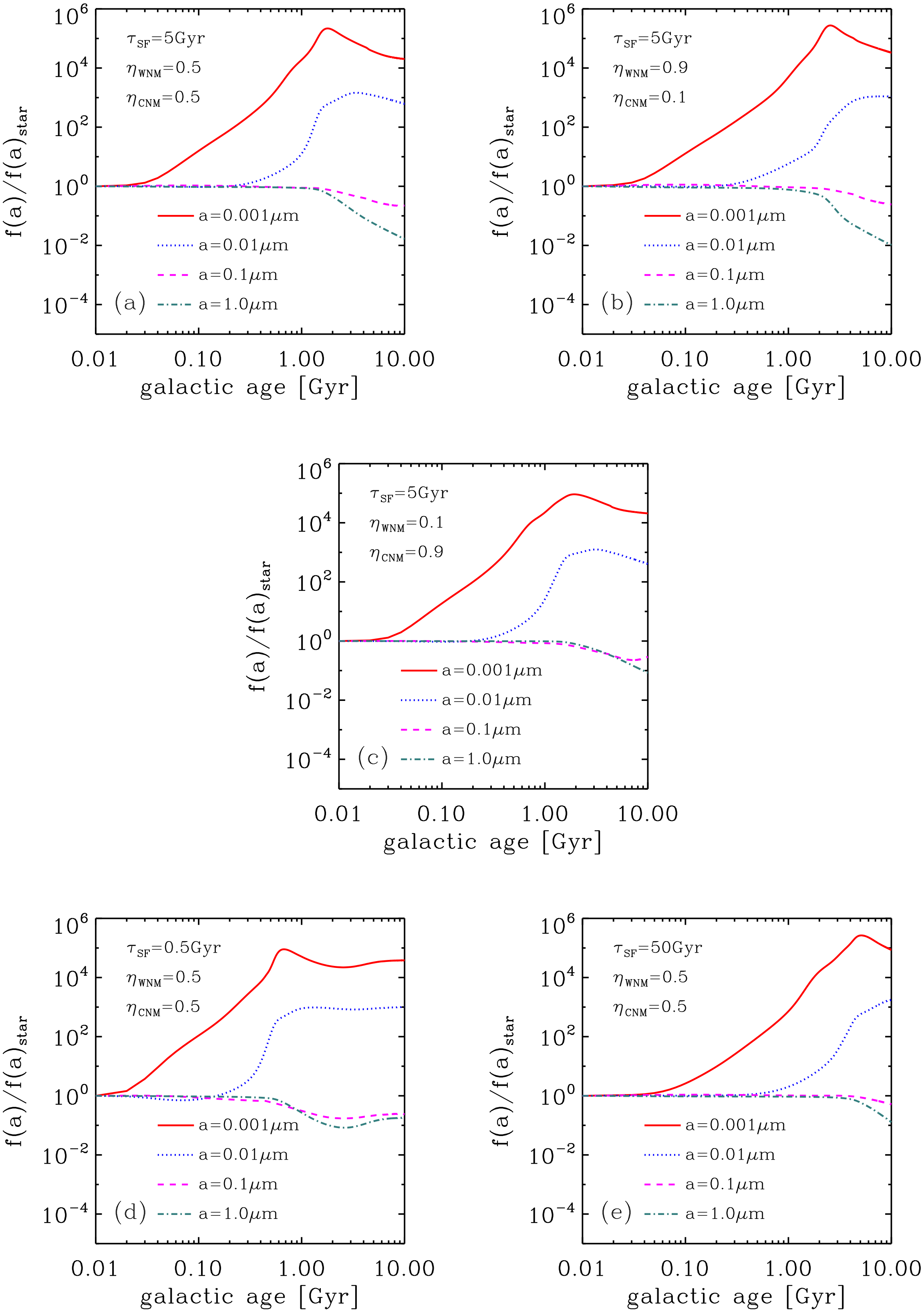

Figure 9. Time evolution of the ratio between the size distribution functions, $f(a)$, and $f(a)_{\rm star}$, the latter being obtained by considering only stellar processes [the first and second terms in right hand size of Eq. (28)]. Panel (a), (b), and (c) are the cases with $(\eta_{\rm WNM}, \eta_{\rm CNM}) = (0.5, 0.5), (0.9, 0.1)$, and $(0.1, 0.9)$, respectively with $\tau_{\rm SF} = 5$ Gyr and $n_{\rm SN} = 1.0$ cm^{-3}. Panel (d) and (e) are the case with $\tau_{\rm SF} = 0.5$ Gyr and 50 Gyr, respectively with $(\eta_{\rm WNM}, \eta_{\rm CNM}) = (0.5, 0.5)$. Solid, dotted, dashed, and dot-dashed lines represent the ratio of $a = 0.001$ μm, 0.01 μm, 0.1 μm, and 1.0 μm, respectively.

we take shattering and coagulation into account, the grain size distribution is modified significantly by these two processes. In particular, shattering indirectly contribute to the large increase of the total dust mass: After small grains ($a \lesssim 0.01$ μm) are produced by shattering, grain growth becomes more effective because of the enhanced surface-to-volume ratio. Furthermore, grain growth produces a large bump in the grain size distribution around $a = 0.01$ μm. The effects of shattering in WNM and CNM on the size distribution appear at different grain radii: While grains with $a > 0.2$ μm are mainly shattered in WNM, shattering in CNM affects grains with $a \sim 0.1$ μm. Furthermore, the effect of shattering, in particular shattering in WNM, is large enough to determine the maximum size of grains in the ISM. Coagulation occurs effectively after the abundance of small grains is enhanced by shattering, and the grain size distribution is deformed to have a bump at a larger size ($a \sim 0.03$–0.05 μm at $t \sim 10$ Gyr) by coagulation. We conclude that the evolution of both the total dust mass and the grain size distribution in galaxies are related strongly to each other and the grain size distribution changes drastically through the galaxy evolution.

ACKNOWLEDGMENTS

We thank the anonymous referee for many suggestions, which were useful to improve the quality and the clarity of this paper. We are grateful to Akio K. Inoue, Takashi Kozasa, Daisuke Yamasawa, and Asao Habe for fruitful discussions, to Satoshi Okuzumi and Hiroshi Kobayashi for helpful discussions on the process of grain–grain collision, to Lars Mattsson for his comments which improve the presentation of this paper and to Jennifer M. Stone for checking the English. RSA acknowledges the hospitality of the members in Institute of Astronomy and Astrophysics, Academia Sinica during his stay. RSA has been supported from the Grant-in-Aid for JSPS Research under Grant No. 23-5514. RSA and TTT have been also partially supported from the Grand-in-Aid for the Global COE Program “Quest for Fundamental Principles in the Universe: from Particles to the Solar System and the Cosmos” from the Ministry of Education, Culture, Sports, Science and Technology (MEXT) of Japan. TTT have been supported by the Grant-in-Aid for the Scientific Research Fund (TTT: 23340046, 24111707) commissioned by the MEXT and by the Strategic Young Researcher Overseas Visits Program for Accelerating Brain Circulation commissioned by the JSPS (R2405). HH is supported by NSC grant 99-2112-M-001-006-MY3. T.N. has been supported by World Premier International Research Center Initiative (WPI Initiative), MEXT, Japan, and by the Grant-in-Aid for Scientific Research of the JSPS (22684004, 23224004).

REFERENCES

Anders, E., & Grevesse, N. 1989, GeCoA, 53, 197
Asano, R. S., Takeuchi, T. T., Hirashita, H., & Inoue, A. K. 2013, Earth, Planets, & Space, 65, 213
Bernard, J. -P. et al. 2008, AJ, 136, 919
Bertelli, G., Bressan, A., Chiosi, C., Fagotto, F., & Nasi, E. 1994, A&AS, 106, 275
Bianchi, S., Schneider, R. 2007, MNRAS, 378, 973
Calura, F., Pipino, A., & Matteucci, F. 2008, A&A, 479, 669
Chokshi, A., Tielens, A. G. G. M., & Hollenbach, D. 1993, ApJ, 407, 806
Draine, B. T. 2009, in Henning Th., Grün E., Steinacker J., eds, Cosmic Dust – Near and Far, ASP Conference Series, ASP, San Francisco, p. 453
Draine, B. T., & Lee, H. M. 1984, ApJ, 285, 89
Dwek, E. & Scalo, J. M. 1980, ApJ, 239, 193
Dwek, E. 1998, ApJ, 501, 643
Evans, A. 1994, The Dusty Universe, Wiley, Chichester
Fitzpatrick, E. L., & Massa, D. 2007, ApJ, 663, 320
Gallerani, S., Maiolino, R., Juarez, Y., Nagao, T., Marconi, A., Bianchi, S., Schneider, R., Mannucci, F., Oliva, T., Willott, C. J., Jiang, L., & Fan, X. 2010, A&A, 523, 85
Gordon, K. D., Clayton, G. C., Misselt, K. A., Landolt, A. U., & Wolff, M. J. 2003, ApJ, 594, 279
Groenewegen, M. A. T. 1997, A&A, 317, 503
Harris, J., & Zaritsky, D. 2009, ApJ, 138, 1243
Heger, A., Fryer, C. L., Woosley, S. E., Langer, N., & Hartmann, D. H. 2003, ApJ, 591, 288
Hirashita, H. 1999a, ApJ, 510, L99
Hirashita, H. 1999b, ApJ, 522, 220
Hirashita, H., & Ferrara, A. 2002, MNRAS, 337, 921
Hirashita, H., Nozawa, T., Kozasa, T., Ishii, T. T., & Takeuchi, T. T. 2005, MNRAS, 357, 1077
Hirashita, H., & Omukai, K. 2009. MNRAS, 399, 1795
Hirashita, H., & Yan, H. 2009, MNRAS, 394, 1061
Hirashita, H. 2010, MNRAS, 407, L49
Hirashita, H., Nozawa, T., Yan, H., & Kozasa, T. 2010, MNRAS, 404, 1448
Hirashita, H. & Kuo, T-M. 2011, MNRAS, 416, 1340
Hirashita, H. 2012, MNRAS, 422, 1263

Ikeuchi, S., & Tomita, H. 1983, PASJ, 35, 77

Inoue, A. K. 2003, PASJ, 55, 901

Inoue, A. K. 2011, EPS, 63, 1

Jones, A. P., Tielens, A. G. G. M., Hollenbach, D. J. & McKee, C. F. 1994, ApJ, 433, 797

Jones, A. P., Tielens, A. G. G. M., Hollenbach, D. J. 1996, ApJ, 469, 740

Jones, A. P., & Nuth, J. A. III. 2011, A&A, 530, 44

Karakas, A. I. 2010, MNRAS, 403, 1413

Kennicutt, R. C. 1998, ApJ, 498, 541

Kim, S.-M., Martin, P. G., & Hendry, P. D. 1994, ApJ, 422, 164

Kobayashi, C., Umeda, H., Nomoto, K., Tominaga, N., & Ohkubo, T. 2006, ApJ, 653, 1145

Koyama, H., & Inutsuka, S. 2002, ApJ, 564, 97

Kozasa, T., Nozawa, T., Tominaga, N., Umeda, H., Maeda, K., Nomoto, K. 2009, in Henning Th., Grün E., Steinacker J., eds, ASP Conf. Ser. Vol. 414, Cosmic Dust Near and Far. Astron. Soc. Pac., San Francisco, p. 43

Kuo, T.-M., & Hirashita, H. 2012, MNRAS, 424, L34

Liffman, K., & Clayton, D. D. 1989, ApJ, 340, 853

Luck, R. E., Moffett, T. J., Barnes, T. G., III, & Gieren, W. P. 1998, AJ, 115, 605

Maiolino, R., Schneider, R., Oliva, E., Bianchi, S., Ferrara, A., Mannucci, F., Pedani, M., & Roca Sogorb, M. 2004, Nat, 431, 533

Mathis, J. S. 1990, ARA&A, 28, 37

Mathis, J. S., Rumpl, W., & Nordsieck, K. H. 1977, ApJ, 217, 425

Matsuura, M., Dwek, E., Meixner, M., et al. 2011, Science, 333, 1258

McKee, C. F., & Ostriker, E. C. 2007, ARA&A, 45, 565

Michałowski, M. J., Murphy, E. J., Hjorth, J., Watson, D., Gall, C., & Dunlop, J. S. 2010, A&A, 522, A15

Nomoto, K., Iwamoto, K., Nakasato, N., Thielemann, F.-K., Brachwitz, F., Tsujimoto, T., Kubo, Y., & Kishimoto, N. 1997, NuPhA, 621, 467

Nozawa, T., Kozasa, T., Umeda, H., Maeda, K., & Nomoto, K. 2003, ApJ, 598, 785

Nozawa, T., Kozasa, T., & Habe, A. 2006, ApJ, 648, 435

Nozawa, T., Kozasa, T., Habe, A., Dwek, E., Umeda, H., Tominaga, N., Maeda, K., & Nomoto, K. 2007, ApJ, 666, 955

Nozawa, T., Kozasa, T., Tominaga, N., Maeda, K., Umeda, H., Nomoto, K., & Krause, O. 2010, ApJ, 713, 356

Nozawa, T., Maeda, K., Kozasa, T., Tanaka, M., Nomoto, K., & Umeda, H. 2011, ApJ, 736, 45

O'Donnell, J. E., & Mathis, J. S. 1997, ApJ, 479, 806

Ormel, C. W., Paszun, D., Dominik, C., & Tielens, A. G. G. M. 2009, A&A, 502, 845

Pei, Y. C. 1992, ApJ, 395, 130

Pipino, A., Fan, X. L., Matteucci, F., Calura, F., Silva, L., Granato, G., & Maiolino, R. 2011, A&A, 525, 61

Raiteri, C. M., Villata, M., & Navarro, J. F. 1996, A&A, 315, 105

Russell, S. C., & Dopita, M. A. 1992, ApJ, 384, 508

Salpeter, E. E. 1955, ApJ, 121, 161

Schmidt, M. 1959, ApJ, 129, 243

Silvia, D. W., Smith, B. D., & Shull, J. M. 2012, ApJ, 748, 12

Spitzer, L. Jr. 1978, Physical Processes in the Interstellar Medium (Wiley, New York) p.207

Stepnik, B., et al. 2003, A&A, 398, 551

Takagi, T., Vansevičius, V., & Arimoto, N. 2003, PASJ, 55, 385

Takeuchi, T. T., Hirashita, H., Ishii, T. T., Hunt, L. K., & Ferrara, A. 2003, MNRAS, 343, 839

Takeuchi, T. T., Ishii, T. T., Nozawa, T., Kozasa, T., & Hirashita, H. 2005, MNRAS, 362, 592

Todini, P., & Ferrara, A. 2001, MNRAS, 325, 726

Valiante, R., Schneider, R., Bianchi, S., Andersen, A. C. 2009, MNRAS, 397, 1661

Valiante, R., Schneider, R., Salvadori, S., & Bianchi, S. 2011, MNRAS, 416, 1916

Weingartner, J. C., & Draine, B. T. 2001, ApJ, 548, 296

Winters, J. M., Fleischer, A. J., Le Bertre, T., & Sedlmayr, E. 1997, A&A, 326, 305

Wolfire, M. G., McKee, C. F., Hollenbach, D., & Tielens, A. G. G. M. 2003, ApJ, 587, 278

Yamasawa, D., Habe, A., Kozasa, T., Nozawa, T., Hirashita, H., Umeda, H., & Nomoto, K. 2011, ApJ, 735, 44

Yan, H., Lazarian, A., & Draine, B. T. 2004, ApJ, 616, 895

Yasuda, Y., & Kozasa, T. 2012, ApJ, 745, 159

Zhukovska, S., Gail, H. P., Trieloff, M. 2008, A&A, 479, 453

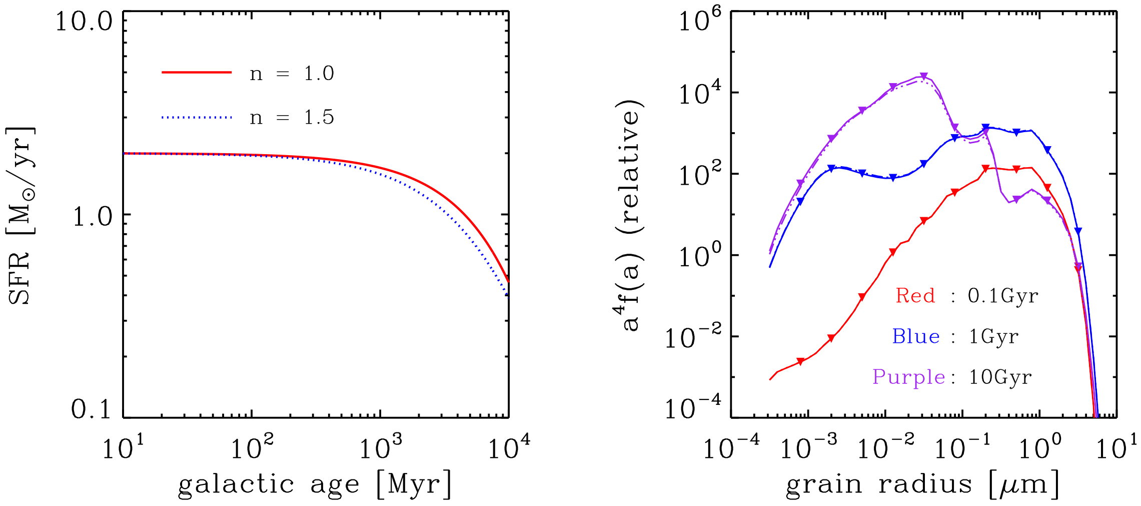

Figure A1. Left panel: the star formation history with $n = 1.0$ (solid line) and 1.5 (dotted line). Right panel: grain size distribution with $n = 1.0$ (triple-dot-dashed line) and 1.5 (solid line with triangles). We adopted $\tau_{\rm SF} = 5$ Gyr, $n_{\rm SN} = 1.0$ cm^{-3}, and $\eta_{\rm WNM} = \eta_{\rm CNM} = 0.5$ in these plots. Note that the red and blue triple-dot-dashed lines overlap with the red and blue solid lines with triangles.

APPENDIX A: EXAMINATION OF PARAMETER DEPENDENCE

In this Appendix, we show dust evolution models with parameters different from the values adopted in the main text.

A1 The Schmidt law index $n = 1.5$

In Fig. A1, we show star formation history (SFH) and the evolution of the grain size distribution with the Schmidt law index $n = 1.0$ and 1.5. To compute the SFH and grain size distribution by using star formation rate with the Schmidt index $n = 1.5$, the SFR with the Schmidt law index $n = 1.5$ (SFR$_{1.5}$) is expressed as

$$\mathrm{SFR}_{1.5}(t) = \frac{M_{\rm ISM}^{1.5}(t)}{\nu_{1.5}}, \tag{A1}$$

where $\nu_{1.5}$ is a constant. We define the value of $\nu_{1.5}$ so that it satisfies the following equation at $t = 0$:

$$\frac{M_{\rm ISM}(t)}{\mathrm{SFR}_{1.5}(t)} = \tau_{\rm SF}. \tag{A2}$$

This is set to compare it with $\tau_{\rm SF}$ for $n = 1$ easily. Thus, we obtain

$$\nu_{1.5} = \tau_{\rm SF} M_{\rm tot}^{0.5}. \tag{A3}$$

From Fig. A1, we find that the results are not significantly different between the cases with the $n = 1.0$ and 1.5.

A2 The index of the Salpeter IMF $q = 1.35$

Figure A2 shows the SFH and the evolution of the grain size distribution with the power-law index of the Salpeter IMF $q = 1.35$ and 2.35 (fiducial value in this paper). We observe that SFRs are almost the same, but the grain size distributions are different. If q is small, that is, a large number of SNe II are produced, the abundance of dust and metals increase earlier than the case with large q. As a result, the dust amount of each size of grains [the values of $a^4f(a)$] with $q = 1.35$ is larger than the case with $q = 2.35$. The dust processes in the ISM also become effective earlier because of the larger dust abundance. However, we find that the trend of the evolution of the grain size distribution (at early phases, stars are dominant sources of dust, as time passes, the processes in the ISM become important) does not change.

APPENDIX B: TIMESCALE OF THE CHANGE OF $F(A)/F(A)_{\rm STAR}$

In Section 4, we found that the timescale of the change of $f(a)/f(a)_{\rm star}$ of all sizes of grains depends on star formation timescale, and the change are due to coagulation for small grains and shattering for large grains. Since both of shattering and coagulation are collisional

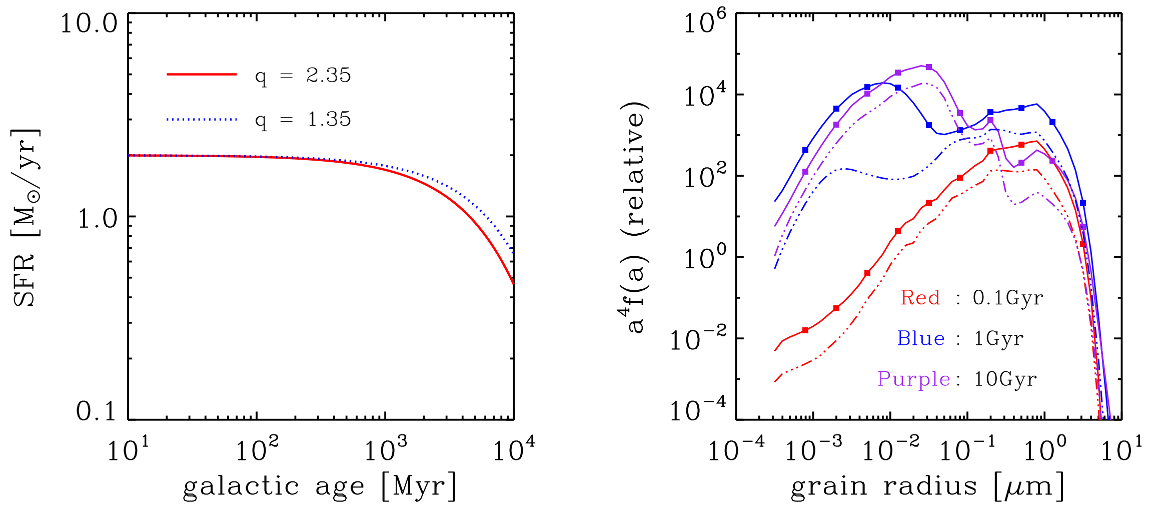

Figure A2. Left panel: the star formation history with $q = 2.35$ (solid line) and 1.35 (dotted line). Right panel: grain size distribution with $q = 2.35$ (triple-dot-dashed lines) and 1.35 (solid lines with filled squares). We adopted $\tau_{\rm SF} = 5$ Gyr, $n_{\rm SN} = 1.0\ {\rm cm}^{-3}$ and $\eta_{\rm WNM} = \eta_{\rm CNM} = 0.5$ in these plots.

processes, the timescales scale with the grain abundance in the same way. In order to evaluate the dependence on the star formation timescale, we compare the contributions of stars and shattering.

First, we consider the stellar contribution [Eq. (29)]. If D is defined as

$$D \equiv \int_0^\infty \int_{m_{\rm cut}(t)}^{100\ {\rm M}_\odot} \Delta m_{\rm d}(m, Z(t-\tau_m), a)\phi(m){\rm d}m{\rm d}a, \tag{B1}$$

with Eq. (4), the stellar contribution can be approximated as

$$\left.\frac{{\rm d}M_{\rm d}}{{\rm d}t}\right|_{\rm star} \simeq D\frac{M_{\rm ISM}}{\tau_{\rm SF}}. \tag{B2}$$

Then, we consider the timescale of shattering, $\tau_{\rm shat}$. Since shattering is a collisional process, $\tau_{\rm shat}$ can be represented as

$$\tau_{\rm shat} \simeq \frac{1}{\pi\langle a^2\rangle v n_{\rm grains}}, \tag{B3}$$

where $\langle a^2\rangle$ is the 2nd moment of a grain size a, v is the relative velocity of grains, and $n_{\rm grain}$ is the number density of grains, which is given by

$$\frac{4}{3}\pi\langle a^3\rangle s n_{\rm grain} \sim \mu n_{\rm H,shat} m_{\rm H}\frac{M_{\rm d}}{M_{\rm ISM}}, \tag{B4}$$

where $\langle a^3\rangle$ is the 3rd moment of a grain size, s is the bulk density of dust grains, $n_{\rm H,shat}$ is the hydrogen number density in the region where shattering occurs, and $m_{\rm H}$ is the mass of the hydrogen atom. We assume the contribution of shattering to the amount of dust grains as $M_{\rm d}/\tau_{\rm shat}$, and comparing this equation with Eq. (B2), we obtain the relation between shattering timescale and star formation timescale,

$$\tau_{\rm shat} \simeq \tau_{\rm SF}\frac{M_{\rm d}}{M_{\rm ISM}}\frac{1}{D}. \tag{B5}$$

In addition, by substituting Eqs. (B3) and (B4) into Eq. (B5), we obtain

$$\tau_{\rm shat} \simeq \sqrt{\frac{\frac{4}{3}\pi\langle a^3\rangle s}{\pi\langle a^2\rangle v\mu m_{\rm H} n_{\rm H,shat} D}}\,\tau_{\rm SF}^{1/2}. \tag{B6}$$

To evaluate this value, we adopt $s = 3.0\ {\rm g\ cm}^{-3}$, $v = 20\ {\rm km\ s}^{-1}$ and $n_{\rm H,shat} = 0.3\ {\rm cm}^{-3}$ (WNM) as a representative value. Also, from our calculation, $D \simeq 10^{-3}$, and $\langle a^3\rangle/\langle a^2\rangle \simeq 10^{-5}$ cm for dust grains produced by stars. Then, we finally obtain

$$\tau_{\rm shat} \sim 1\left(\frac{\tau_{\rm SF}}{\rm Gyr}\right)^{\frac{1}{2}}\ [{\rm Gyr}]. \tag{B7}$$

Thus, we conclude that the timescale of shattering, that is, the timescale of the change of $f(a)/f(a)_{\rm star}$, is proportional to $\tau_{\rm SF}^{1/2}$.

This paper has been typeset from a TEX/ LATEX file prepared by the author.